Time-reversal symmetric Kitaev model and topological superconductor in two dimensions

R. Nakai, S. Ryu, and A. Furusaki

Phys. Rev. B **85**, 155119 — Published 11 April 2012

DOI: 10.1103/PhysRevB.85.155119

Time-reversal symmetric Kitaev model and topological superconductor in two dimensions

R. Nakai,[1] S. Ryu,[2] and A. Furusaki[3]

[1] *Department of Physics, University of Tokyo, Tokyo 113-0033, Japan**
[2] *Department of Physics, University of Illinois, 1110 West Green St, Urbana IL 61801*
[3] *Condensed Matter Theory Laboratory, RIKEN, Wako, Saitama 351-0198, Japan*

(ΩDated: March 27, 2012)

A time-reversal invariant Kitaev-type model is introduced in which spins (Dirac matrices) on the square lattice interact via anisotropic nearest-neighbor and next-nearest-neighbor exchange interactions. The model is exactly solved by mapping it onto a tight-binding model of free Majorana fermions coupled with static $\mathbb{Z}_2$ gauge fields. The Majorana fermion model can be viewed as a model of time-reversal invariant superconductor and is classified as a member of symmetry class DIII in the Altland-Zirnbauer classification. The ground-state phase diagram has two topologically distinct gapped phases which are distinguished by a $\mathbb{Z}_2$ topological invariant. The topologically nontrivial phase supports both a Kramers' pair of gapless Majorana edge modes at the boundary and a Kramers' pair of zero-energy Majorana states bound to a 0-flux vortex in the π-flux background. Power-law decaying correlation functions of spins along the edge are obtained by taking the gapless Majorana edge modes into account. The model is also defined on the one-dimension ladder, in which case again the ground-state phase diagram has $\mathbb{Z}_2$ trivial and non-trivial phases.

PACS numbers: 75.10.Jm, 73.43.-f, 75.10.Kt

I. INTRODUCTION

Topological phases are a gapped state of matter which does not fall into a conventional characterization of condensed matter systems in terms of symmetry breaking. The prime and classic example is the fractional quantum Hall effect which is realized in two-dimensional electron gas under strong magnetic field. Topological phases in the fractional quantum Hall effect are characterized, e.g., by the presence of (chiral) edge states, by a set of fractionally charged quasiparticles which obey fractional or non-Abelian statistics, and also by the topological ground state degeneracy when a system is put on a spatial manifold with non-trivial topology.[1] A fractional quantum Hall state cannot be adiabatically deformed into a trivial state of matter such as an ordinary band insulator.

While it is necessary to break time-reversal symmetry (TRS) to realize the fractional quantum Hall effect, a topological phase can exist without breaking TRS, as seen in several examples of gapped quantum spin liquid states (e.g., $\mathbb{Z}_2$ spin liquid states). Furthermore, a phase which is not topological, in the sense that it can be adiabatically connected to a trivial phase (vacuum), can still be topologically distinct from the vacuum once we impose some discrete symmetries, such as TRS; such phases can be called symmetry protected topological phase.[2–4]

Symmetry protected topological phases are recently realized in the discovery of non-interacting topological band insulators, such as the quantum spin Hall effect and the three-dimensional topological insulator;[5,6] If we enforce TRS, these band insulators cannot be adiabatically connected to a trivial band insulator, as seen from the presence of edge or surface states. Phases of non-interacting fermion systems (including Bogoliubov-de Genne quasiparticles in the presence of meanfield BCS pairing gap) have been fully classified in terms of presence or absence of discrete symmetries of various kind for arbitrary spatial dimensions.[7–9]

Studies on realizations of strongly interacting counterparts of these time-reversal symmetric topological band insulators, i.e., "the fractional topological insulator," are still in their early stage.[10]

The notion of symmetry protected topological phases is not limited to electron systems with TRS, but applies to bosonic systems including quantum spin systems.[2] The Haldane phase in integer spin chains has been known as an example of a gapped spin liquid phase in one spatial dimension with a localized end state which carries half-integer spin. It is recently uncovered that the Haldane phase has a symmetry protected topological order.[3,4]

The list of experimentally established realizations of strongly interacting topological phases is still limited. However, a number of exactly solvable models have been proposed, helping us to deepen our understanding of the topological orders in many-body systems. Examples are the AKLT model,[11] the quantum dimer models,[12] the toric code model,[13] and the string-net models,[14] etc. In Ref. 15, Kitaev introduced an exactly solvable quantum spin model on the two-dimensional honeycomb lattice. A central feature of the honeycomb lattice Kitaev model, among others, is that it realizes, in the absence of TRS, a gapped phase with a chiral Majorana edge state, and non-Abelian anyonic excitations in the bulk. Variants of the Kitaev model, such as SU(2) invariant models,[16,17] have been studied recently.[18]

In this paper, we consider an extension of the Kitaev model on the square lattice that respects a TRS of some sort. Following similar extensions of the Kitaev model on the three-dimensional diamond lattice[19,20] and on the two-dimensional square lattice,[21] we consider

two spin-1/2 degrees of freedom on each site that compose 4×4 Dirac matrices (γ matrices). Similarly to the original Kitaev model, we consider interactions among spins which are anisotropic in space and are designed in such a way that the model is solvable through the (Majorana) fermion representation of spins. Written in terms of the fermions, our model belongs to the symmetry class DIII in the Altland-Zirnbauer classification of free fermions.[7,22] Symmetry class DIII is a class of fermions which are subjected to TRS, and also to particle-hole symmetry [i.e., a Majorana (or real) condition]. This should be contrasted with the original Kitaev model, which when rewritten in terms of Majorana fermions, belongs to symmetry class D, which is a class of Majorana (real) fermions without TRS. One of our main findings is a topological phase which is characterized by the $\mathbb{Z}_2$ topological invariant of class DIII in the bulk, and supports gapless *non-chiral* Majorana fermion edge modes which form a Kramers pair: the Bloch wavefunctions of the "emergent" Majorana fermions in this phase are in the same topological class as those of fermionic quasiparticles in the topological superconductor in symmetry class DIII. This phase is a time-reversal symmetric analogue of the non-Abelian phase of the honeycomb lattice Kitaev model, and in fact, the model can be viewed as a "doubled" version of the original Kitaev model; just like the quantum spin Hall system with non-trivial $\mathbb{Z}_2$ topological invariant can be constructed from two copies of the integer quantum Hall systems with opposite chiralities. From this point of view, our model is somewhat analogous to time-reversal invariant "doubled" anyon models discussed in Ref. 23.

This paper is organized as follows. In Sec. II, Hamiltonian with nearest-neighbor and next-nearest-neighbor interactions is presented in terms of Dirac matrices and transformed to free Majorana Hamiltonian that respects TRS. The symmetry class in the Altland-Zirnbauer classification is specified, and the phase diagram of the ground states is obtained. In Sec. III, we show by numerical calculation and a topological argument that the helical Majorana edge modes appear in the phase with a nontrivial $\mathbb{Z}_2$ topological invariant. In Sec. IV, some spin correlation functions are calculated along the edge. The existence of the gapless Majorana edge modes determines the power-law decay of the correlation functions. In Sec. V, we confirm that an isolated vortex excitation of the $\mathbb{Z}_2$ gauge field hosts a time-reversal pair of zero-energy Majorana bound states. In Sec. VI, we study the model on one-dimensional lattice. Two distinct phases are found which are characterized by the $\mathbb{Z}_2$ topological invariant. In Appendix we give an alternative representation of Dirac matrices in terms of Jordan-Wigner fermions which keeps the same four-dimensional Hilbert space at each site.

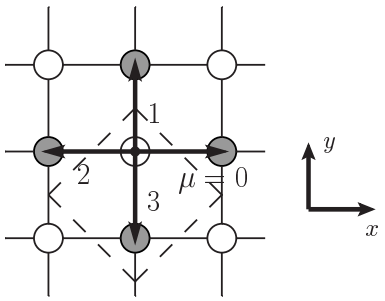

FIG. 1. Square lattice and link vectors $\boldsymbol{e}_\mu$ with $\mu = 0, 1, 2, 3$ emanating from a site on the A-sublattice (open circle) to a neighboring site on the B-sublattice (filled circle). The dashed lines indicate a unit cell.

II. MODEL

In this section, we introduce an extension of the Kitaev model that respects time-reversal symmetry. The Hamiltonian is written in terms of Dirac matrices defined on each site of the two-dimensional square lattice. We first consider the Hamiltonian with nearest-neighbor couplings only and show that its ground-state phase diagram has a gapped phase and a gapless phase.[24] We then add next-nearest-neighbor couplings to the Hamiltonian, which open a gap in the gapless phase. This gapped phase can be viewed as a topological superconducting phase when the Hamiltonian is transformed to a free Majorana tight-binding Hamiltonian. The time reversal symmetry is preserved in both of the gapped phases.

A. Hamiltonian with nearest-neighbor interactions only

There are a class of exactly solvable quantum spin models in which Ising-type nearest-neighbor exchange interactions have different easy-axis directions for each link on the lattice. In the original Kitaev model on the honeycomb lattice,[15] three components of the Pauli matrices are assigned to the three links emanating from a site of the honeycomb lattice. Similarly, to define an exactly solvable spin model on the square lattice, we can take Dirac matrices and assign four components of the Dirac matrices to four distinct types of links that emanate from each site, as in the Kitaev-type model on the diamond lattice.[19]

The sites on the square lattice are divided into A- and B-sublattices. Four links from a site on the A-sublattice are labeled, respectively, by $\mu = 0, 1, 2, 3$ counterclockwise from the positive x-direction (Fig. 1). Taking the lattice constant $a_0 = 1$, four types of link vectors $\boldsymbol{e}_\mu$ are written in the two-dimensional coordinate as

$$\boldsymbol{e}_0 = \begin{pmatrix} 1 \\ 0 \end{pmatrix}, \ \boldsymbol{e}_1 = \begin{pmatrix} 0 \\ 1 \end{pmatrix}, \ \boldsymbol{e}_2 = \begin{pmatrix} -1 \\ 0 \end{pmatrix}, \ \boldsymbol{e}_3 = \begin{pmatrix} 0 \\ -1 \end{pmatrix}, \quad (1)$$

where the direction of each vector is chosen from a site of the A-sublattice to a neighboring site of the B-sublattice. In the following the links labelled by $\mu(=0,1,2,3)$ are referred to as "μ-links".

For each site on the square lattice, we consider a four-dimensional bosonic Hilbert space. The four-dimensional Hilbert space can be considered as that of a spin-3/2 operator,[21] or the direct product of spin-1/2 degrees of freedom and two orbital degrees of freedom. To describe the local bosonic Hilbert space, we define a set of Dirac matrices α in terms of the γ matrices in the standard manner:[25]

$$\alpha^0 = \gamma^0, \quad \alpha^a = \gamma^0\gamma^a \quad (a=1,2,3). \tag{2}$$

The Dirac matrices α satisfy the anticommutation relations $\{\alpha^\mu, \alpha^\nu\} = 2\delta^{\mu\nu}$, while the γ matrices satisfy $\{\gamma^\mu, \gamma^\nu\} = 2g^{\mu\nu}$, where $g^{\mu\nu} = \mathrm{diag}(1,-1,-1,-1)$. With the fifth component of the γ matrices, $\gamma^5 = i\gamma^0\gamma^1\gamma^2\gamma^3$, we define another set of Dirac matrices ζ,

$$\zeta^0 = \gamma^5, \quad \zeta^a = \gamma^5\gamma^a \quad (a=1,2,3). \tag{3}$$

The ζ matrices also satisfy the anticommutation relations $\{\zeta^\mu, \zeta^\nu\} = 2\delta^{\mu\nu}$. We represent the γ matrices as the direct product of two Pauli matrices σ^i and τ^i (the Dirac representation),

$$\gamma^0 = \sigma^0 \otimes \tau^3, \quad \gamma^a = i\sigma^a \otimes \tau^2 \quad (a=1,2,3), \tag{4}$$

where σ^0 and τ^0 are 2×2 unit matrices. The two sets of Dirac matrices are then written as

$$\alpha^\mu : \alpha^0 = \sigma^0 \otimes \tau^3, \quad \alpha^a = \sigma^a \otimes \tau^1 \quad (a=1,2,3), \tag{5}$$

$$\zeta^\mu : \zeta^0 = \sigma^0 \otimes \tau^1, \quad \zeta^a = -\sigma^a \otimes \tau^3 \quad (a=1,2,3). \tag{6}$$

We introduce the nearest-neighbor spin Hamiltonian,

$$\mathcal{H}_0 = -\sum_{\mu=0}^{3} J_\mu \sum_{\mu\text{-links}} (\alpha_j^\mu \alpha_k^\mu + \zeta_j^\mu \zeta_k^\mu), \tag{7}$$

where J_μ is the coupling constant on μ-links. The subscripts j and k refer to nearest-neighbor sites on the A- and B-sublattice, respectively, which are connected by a μ-link. That is, the position vectors of the sites j and k, $\boldsymbol{r}_j$ and $\boldsymbol{r}_k$, are related by $\boldsymbol{r}_k = \boldsymbol{r}_j + \boldsymbol{e}_\mu$. Without loss of generality, we can assume $J_\mu \geq 0$. In terms of the two Pauli matrices σ^μ and τ^μ, the model can be written as

$$\mathcal{H}_0 = -\sum_{\mu=0}^{3} J_\mu \sum_{\mu\text{-links}} (\sigma_j^\mu \sigma_k^\mu)(\tau_j^3 \tau_k^3 + \tau_j^1 \tau_k^1). \tag{8}$$

While the part of the exchange term involving the σ-matrices is anisotropic, the part involving the τ-matrices is isotropic and XY like; the model has a U(1) symmetry rotating the τ-matrices around the τ^2 axis. This U(1) symmetry, however, will be lost when we later perturb the nearest neighbor model (7).

The model is also invariant under a kind of time-reversal symmetry operation which is designed to become a time-reversal symmetry operation for half-integer spin fermions in the Majorana representation discussed later. Let us first consider a time-reversal operation T defined by

$$T = (i\sigma^2) \otimes (i\tau^2)\mathcal{K},$$
$$T\sigma^a T^{-1} = -\sigma^a, \quad T\tau^a T^{-1} = -\tau^a, \tag{9}$$

with complex conjugation operator $\mathcal{K}$ and $a = 1,2,3$. Note that $T^2 = +1$. Under T, α and ζ are transformed as

$$T\alpha^\mu T^{-1} = -\alpha_\mu, \quad T\zeta^\mu T^{-1} = -\zeta_\mu,$$
$$Ti\gamma^5\gamma^0 T^{-1} = -i\gamma^5\gamma^0, \tag{10}$$

where covariant and contravariant vectors are defined as $\alpha^\mu = (\alpha^0, \alpha^a)$ and $\alpha_\mu = (\alpha^0, -\alpha^a)$. As we have noted, while the σ-part of our Hamiltonian is fully anisotropic in σ space, the τ-part of the Hamiltonian is invariant under a rotation around τ^2 axis. In particular, it is invariant under a rotation R by $\pi/2$ around τ^2 axis,

$$R\begin{pmatrix}\tau^1\\ \tau^2\\ \tau^3\end{pmatrix}R^{-1} = \begin{pmatrix}\tau^3\\ \tau^2\\ -\tau^1\end{pmatrix}, \quad R = \frac{\tau^0 + i\tau^2}{\sqrt{2}}. \tag{11}$$

Under R, α and ζ are transformed as

$$R\alpha^\mu R^{-1} = -\zeta^\mu, \quad R\zeta^\mu R^{-1} = +\alpha^\mu,$$
$$Ri\gamma^5\gamma^0 R^{-1} = +i\gamma^5\gamma^0. \tag{12}$$

By combining T with R we can define yet another antiunitary operation, $T' = RT$,

$$T' = RT = \frac{1}{\sqrt{2}}(i\tau^2 - \tau^0)i\sigma^2\mathcal{K},$$
$$T'\sigma^a T'^{-1} = -\sigma^a, \quad T'\begin{pmatrix}\tau^1\\ \tau^2\\ \tau^3\end{pmatrix}T'^{-1} = \begin{pmatrix}-\tau^3\\ -\tau^2\\ +\tau^1\end{pmatrix}. \tag{13}$$

Below, with a slight abuse of language, we will call this operation T' time-reversal operation. When applied to α and ζ,

$$T'\alpha^\mu T'^{-1} = +\zeta_\mu, \quad T'\zeta^\mu T'^{-1} = -\alpha_\mu,$$
$$T'i\gamma^5\gamma^0 T'^{-1} = -i\gamma^5\gamma^0, \tag{14}$$

i.e., time-reversal operation T' exchanges α and ζ, and covariant and contravariant vectors. Notice that

$$T'^2 = i\tau^2, \quad T'^4 = -1. \tag{15}$$

We will impose the time-reversal symmetry T' throughout the paper.

The Hamiltonian (7) has the integrals of motion defined for each plaquette p,

$$W_p = \prod_{(j,k)\in p} \alpha_j^\mu \alpha_k^\mu = \prod_{(j,k)\in p} \zeta_j^\mu \zeta_k^\mu, \tag{16}$$

where (j,k) are the four links on the boundary of a plaquette p, and the sites j and k are on the A- and B-sublattices, respectively.

B. Mapping to Majorana fermion model

The honeycomb lattice Kitaev model can be mapped to a Majorana fermion problem in the presence of a $\mathbb{Z}_2$ gauge field by representing the Pauli matrices in terms of four Majorana fermions per site.[15] Similarly, we can represent the two sets of Dirac matrices α^μ and ζ^μ with six Majorana fermions λ^p $(p = 0, \cdots, 5)$:[14,19–21]

$$\alpha^\mu = i\lambda^\mu\lambda^4, \;\; \zeta^\mu = i\lambda^\mu\lambda^5, \tag{17}$$

where we have not written the site indices explicitly. The Majorana fermions satisfy $(\lambda^p)^\dagger = \lambda^p$ and $\{\lambda^p, \lambda^{p'}\} = 2\delta^{pp'}$. The bosonic Hamiltonian (7) is then mapped to, by using the relation (17), a Majorana Hamiltonian

$$\mathcal{H}_0 = i\sum_{\mu=0}^{3} J_\mu \sum_{\mu\text{-links}} u_{jk}^\mu(\lambda_j^4\lambda_k^4 + \lambda_j^5\lambda_k^5), \tag{18}$$

where $u_{jk}^\mu = i\lambda_j^\mu\lambda_k^\mu$ are defined on the μ-link connecting two neighboring sites j and k which belong to the A- and B-sublattices, respectively. We will use simplified notation u_{jk} for u_{jk}^μ since μ is uniquely determined by the neighboring sites j and k. The identity $(u_{jk})^2 = 1$ implies that the eigenvalue of u_{jk} takes ± 1. The u_{jk} defined on each link of the square lattice are $\mathbb{Z}_2$ gauge fields.

Since u_{jk} commute with each other and also with the Hamiltonian (18), all u_{jk} and the Hamiltonian can be diagonalized simultaneously. Hence the total Hilbert space $\mathcal{L}$ for Majorana fermions is decomposed into subspaces $\mathcal{L}_{\{u_{jk}\}}$ which are specified by the configurations of the eigenvalues of $\mathbb{Z}_2$ gauge fields u_{jk} on every link,

$$\mathcal{L} = \oplus\mathcal{L}_{\{u_{jk}\}}. \tag{19}$$

Within each subspace, the Hamiltonian is regarded as a free Majorana fermion Hamiltonian, where u_{jk} are replaced by their eigenvalue ± 1.

According to Lieb's theorem,[26] the energy of the free Majorana Hamiltonian (18) is minimized when $\mathbb{Z}_2$ gauge fields u_{jk} are such that each plaquette has a π-flux,

$$\prod_{(j,k)\in p} u_{jk} = -1. \tag{20}$$

The left-hand side of Eq. (20), which we denote $\widetilde{W}_p$, is the Majorana fermion representation of the plaquette operator W_p in Eq. (16) and is $\mathbb{Z}_2$ gauge invariant. The condition (20) is satisfied, for example, by setting $u_{jk} = -1$ on the 0-links and $u_{jk} = +1$ on the other links. However, there is redundancy in the choice of $\mathbb{Z}_2$ gauge-field configuration for a given flux configuration.

The time-reversal operation for Dirac matrices [Eq. (14)] is translated into that for Majorana fermions as

$$T'\begin{pmatrix}\lambda^0\\ \lambda^a\end{pmatrix}T'^{-1} = \begin{pmatrix}\lambda^0\\ -\lambda^a\end{pmatrix}, \;\; T'\begin{pmatrix}\lambda^4\\ \lambda^5\end{pmatrix}T'^{-1} = \begin{pmatrix}-\lambda^5\\ \lambda^4\end{pmatrix} \tag{21a}$$

or

$$T'\begin{pmatrix}\lambda^0\\ \lambda^a\end{pmatrix}T'^{-1} = \begin{pmatrix}-\lambda^0\\ \lambda^a\end{pmatrix}, \;\; T'\begin{pmatrix}\lambda^4\\ \lambda^5\end{pmatrix}T'^{-1} = \begin{pmatrix}\lambda^5\\ -\lambda^4\end{pmatrix}. \tag{21b}$$

In order to keep the $\mathbb{Z}_2$ gauge operators invariant under time-reversal transformation, we employ the two types of time-reversal rules to Majorana fermions on each sublattice separately, i.e., Eq. (21a) for the A-sublattice and Eq. (21b) for the B-sublattice.

C. Projection

The Majorana fermion representation (17) preserves the commutation and anticommutation relations of the Dirac matrices α and ζ. However, on each site, the original four-dimensional Hilbert space is doubled in the Majorana fermion representation which employs six flavors of Majorana fermions (or, equivalently, three complex fermions), as in the original Kitaev model.[15] This redundancy can be removed by imposing the condition at every site l on the square lattice,

$$D_l := i\prod_{p=0}^{5}\lambda_l^p = +1. \tag{22}$$

The operator D_l is the Majorana fermion representation of $i\gamma_l^0\gamma_l^1\gamma_l^2\gamma_l^3\gamma_l^5$ that is a unit matrix by definition of the γ matrices. The condition (22) is implemented by the projection operator

$$P = \prod_l \frac{1}{2}(1 + D_l) \tag{23}$$

acting on the states of the Majorana Hamiltonian. (In Appendix an alternative representation of Dirac matrices is given in terms of Jordan-Wigner fermions which is free from the redundancy.)

Now we show that the projection operator (23) eliminates the arbitrariness of the choice of the $\mathbb{Z}_2$ gauge field for a given flux configuration $\{\widetilde{W}_p\}$. Let $|\Psi;\{u_{jk}\}\rangle$ be an eigenstate of Hamiltonian (18) with a $\mathbb{Z}_2$ gauge-field configuration $\{u_{jk}\}$. It follows from the relation

$$[\mathcal{H}_0, D_l] = [\widetilde{W}_p, D_l] = 0, \tag{24}$$

that $D_l|\Psi;\{u_{jk}\}\rangle$ is also an eigenstate of $\mathcal{H}_0$ with the same flux configuration $\{\widetilde{W}_p\}$, but with a different $\mathbb{Z}_2$ gauge-field configuration where the $\mathbb{Z}_2$ gauge fields on the four links around the site l are multiplied by -1. This can be seen from the relations

$$\{u_{jk}, D_j\} = \{u_{jk}, D_k\} = 0, \tag{25}$$

$$[u_{jk}, D_l] = 0 \quad (l \neq j, k). \tag{26}$$

Furthermore, we can consider states generated by acting D_l on multiple sites,

$$\prod_{l\in S} D_l|\Psi;\{u_{jk}\}\rangle, \tag{27}$$

where S is a set of sites from the square lattice. One might think that the total number of such states is $2^{N_{\rm tot}}$, where $N_{\rm tot}$ is the total number of the lattice sites, since $(D_l)^2=1$. However, under the periodic boundary condition, the number of $\mathbb{Z}_2$ gauge-field configurations $\{u_{jk}\}$ generated in this way turns out to be $2^{N_{\rm tot}-1}$, since the product of D_l on the all sites,

$$\prod_l D_l \propto \prod_{(jk)} u_{jk} \prod_l i\lambda_l^4\lambda_l^5, \tag{28}$$

does not change the $\mathbb{Z}_2$ gauge-field configurations. Moreover, eigenstates of the free Majorana fermion Hamiltonian are invariant under the action of (28) up to an overall sign, as creation/annihilation operators of single-particle states anticommute with (28). Obviously, the states generated by acting D_l from distinct sets S and S' are orthogonal,

$$\langle\Psi;\{u_{jk}\}|\prod_{l\in S} D_l \prod_{l'\in S'} D_{l'}|\Psi;\{u_{jk}\}\rangle = 0, \tag{29}$$

unless $S=S'$ or S' is the complementary set of S, since the eigenvalues of the $\mathbb{Z}_2$ gauge-field operators are different between two states. Hence, the states of the form (27) form $2^{N_{\rm tot}-1}$-dimensional orthonormal basis states. Meanwhile, the number of flux configurations is $2^{N_{\rm tot}-1}$, since the total flux must be unity ($\prod_p \widetilde{W}_p = 1$). Considering the fact that there are two additional, independent integrals of motion defined on two closed loops C_x, C_y going around in the x- and y-directions,

$$\widetilde{W}_x = \prod_{(j,k)\in C_x} \alpha_j^\mu \alpha_k^\mu, \tag{30a}$$

$$\widetilde{W}_y = \prod_{(j,k)\in C_y} \alpha_j^\mu \alpha_k^\mu, \tag{30b}$$

we find that the number of $\mathbb{Z}_2$ gauge-field configurations for a given local flux configuration ($\{\widetilde{W}_p\}$) and global flux configurations ($\{\widetilde{W}_x,\widetilde{W}_y\}$), is $2^{2N_{\rm tot}}/(2^{N_{\rm tot}-1}2^2) = 2^{N_{\rm tot}-1}$. Therefore the states (27) exhaust the eigenstates for all $\mathbb{Z}_2$ gauge-field configurations with the same flux configuration. Finally, projecting the state (27) yields

$$P\prod_{l\in S} D_l|\Psi;\{u_{jk}\}\rangle = P|\Psi;\{u_{jk}\}\rangle, \tag{31}$$

since $(1+D_j)D_j = 1+D_j$. Equation (31) implies that the projected state is independent of $\mathbb{Z}_2$ gauge choice. Whatever $\mathbb{Z}_2$ gauge configuration is taken for a given flux configuration, the same set of states are obtained after the projection; any redundant state of the free Majorana fermion Hamiltonian disappears after the projection. Furthermore, we can conclude that matrix elements (for the projected states) of gauge-invariant observables can be calculated by using eigenstates of Majorana fermions with any particular $\mathbb{Z}_2$ gauge configuration.

D. Phase diagram of the nearest-neighbor spin Hamiltonian

Let us set $u_{jk}=-1$ on every 0-link and $u_{jk}=+1$ on the other links of the square lattice, to satisfy the π-flux condition, Eq. (20). This $\mathbb{Z}_2$ gauge-field configuration, which we denote by a four-vector $u^\mu=(u^0,u^1,u^2,u^3)=(-1,1,1,1)$, preserves lattice translation symmetry with the unit cell shown in Fig. 1. We introduce Fourier transformation of Majorana fermion operators on the A-sublattice,

$$a_{\boldsymbol{q}}^s = \frac{1}{\sqrt{2N}}\sum_{j\in{\rm A}} e^{-i\boldsymbol{q}\cdot\boldsymbol{r}_j}\lambda_j^s \qquad (s=4,5), \tag{32a}$$

and of those on the B-sublattice,

$$b_{\boldsymbol{q}}^s = \frac{1}{\sqrt{2N}}\sum_{k\in{\rm B}} e^{-i\boldsymbol{q}\cdot\boldsymbol{r}_j}\lambda_k^s \qquad (s=4,5), \tag{32b}$$

where N is the number of unit cells, and $\boldsymbol{r}_j$ in both of Eqs. (32) is the position vector of the site j on the A-sublattice. That is, $\boldsymbol{r}_j$ in Eq. (32b) is related to the position vector of the site k on the B-sublattice by $\boldsymbol{r}_j = \boldsymbol{r}_k + \boldsymbol{e}_1$. The inverse Fourier transform of Eqs. (32) is given by

$$\lambda_{j\in{\rm A}}^s \equiv a_{\boldsymbol{r}}^s = \sqrt{\frac{2}{N}}\sum_{\boldsymbol{q}} e^{i\boldsymbol{q}\cdot\boldsymbol{r}_j} a_{\boldsymbol{q}}^s, \tag{33a}$$

$$\lambda_{k\in{\rm B}}^s \equiv b_{\boldsymbol{r}}^s = \sqrt{\frac{2}{N}}\sum_{\boldsymbol{q}} e^{i\boldsymbol{q}\cdot(\boldsymbol{r}_k+\boldsymbol{e}_1)} b_{\boldsymbol{q}}^s, \tag{33b}$$

where the wave vector $\boldsymbol{q}$ is in the first Brillouin zone, $|q_x|+|q_y|\le\pi$. The fermion operators defined in Eqs. (32) satisfy the following relations:

$$a_{-\boldsymbol{q}}^s = \left(a_{\boldsymbol{q}}^s\right)^\dagger, \qquad b_{-\boldsymbol{q}}^s = \left(b_{\boldsymbol{q}}^s\right)^\dagger, \tag{34a}$$

$$\{a_{\boldsymbol{q}}^s, a_{\boldsymbol{q}'}^{s'}\} = \{b_{\boldsymbol{q}}^s, b_{\boldsymbol{q}'}^{s'}\} = \delta_{\boldsymbol{q}+\boldsymbol{q}',0}\delta_{s,s'}, \quad \{a_{\boldsymbol{q}}^s, b_{\boldsymbol{q}'}^{s'}\} = 0. \tag{34b}$$

One can thus regard $a_{\boldsymbol{q}}^s$ and $a_{-\boldsymbol{q}}^s$ ($b_{\boldsymbol{q}}^s$ and $b_{-\boldsymbol{q}}^s$) as annihilation and creation operators of fermions (or vice versa). Hamiltonian (18) is written in the momentum space as

$$\mathcal{H}_0 = \sum_{\boldsymbol{q}} \left[i\Phi(\boldsymbol{q})\left(a_{-\boldsymbol{q}}^4 b_{\boldsymbol{q}}^4 + a_{-\boldsymbol{q}}^5 b_{\boldsymbol{q}}^5\right) - i\Phi^*(\boldsymbol{q})\left(b_{-\boldsymbol{q}}^4 a_{\boldsymbol{q}}^4 + b_{-\boldsymbol{q}}^5 a_{\boldsymbol{q}}^5\right)\right], \tag{35}$$

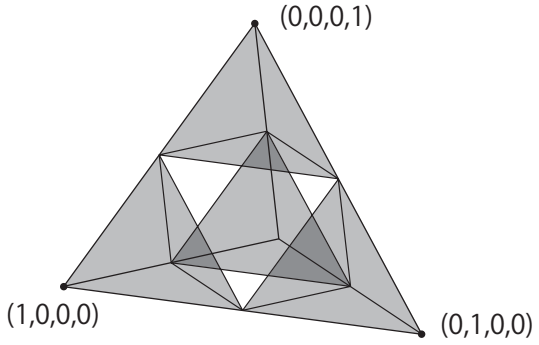

FIG. 2. Phase diagram in the parameter space (J_0, J_1, J_2, J_3). Shaded regions are gapped phases and the other area is gapless phase.

where

$$\Phi(\boldsymbol{q}) = e^{iq_y}\sum_{\mu} J_\mu u^\mu e^{i\boldsymbol{q}\cdot\boldsymbol{e}_\mu} = e^{iq_y}(-J_0 e^{iq_x} + J_1 e^{iq_y} + J_2 e^{-iq_x} + J_3 e^{-iq_y}). \tag{36}$$

The eigenvalues of (35) are $E = \pm|\Phi(\boldsymbol{q})|$. Each eigenstate is doubly degenerate, since λ^4 and λ^5 are decoupled in the Hamiltonian. The ground state is obtained by filling all the eigenstates with negative energy.

The ground-state phase diagram is drawn in Fig. 2, where for illustration purpose we normalized the parameters $\boldsymbol{J} = (J_0, J_1, J_2, J_3)$ such that $J_0 + J_1 + J_2 + J_3 = 1$, $J_\mu \geq 0$. The vertices of the (large) tetrahedron in Fig. 2, $\boldsymbol{J} = (1,0,0,0), (0,1,0,0), (0,0,1,0), (0,0,0,1)$, correspond to the parameter sets in which one of the four coupling constants is much stronger than the others. On the edges of the tetrahedron the sum of two coupling constants is equal to 1. The four shaded regions (smaller tetrahedrons) in Fig. 2 are gapped phases in which there is an energy gap between positive energy bands and negative energy bands. The region including the isotropic point $\boldsymbol{J} = (1/4, 1/4, 1/4, 1/4)$ (the non-shaded part in Fig. 2) is a gapless phase where the positive and negative energy bands touch at two Dirac points, around which Majorana fermions have linear energy dispersions. The gapless phase will become a gapped topological phase, once an energy gap is opened by some perturbations, as is the case in the Kitaev model. On the boundary between a gapped phase and the gapless phase, two Dirac points merge to become a single point in the Brillouin zone. This happens when one of the four J_μ's is equal to the sum of the other three J_μ's.

E. Hamiltonian with next-nearest-neighbor interaction

We add, to the Hamiltonian $\mathcal{H}_0$, perturbations of the form of a product of Dirac matrices from three neighboring sites. As we will see, these perturbations will open a gap at the Dirac points in the gapless phase.

Consider three neighboring sites j, k, and l of a single plaquette shown in Fig. 3, where the sites j and k belong to the same sublattice (either A or B). We consider three-site interaction Hamiltonian of the form

$$\mathcal{H}_z = \sum_{(jlk)} iK^z_{jlk}(\alpha^\mu_j\alpha^\mu_l\alpha^\nu_l\alpha^\nu_k - \zeta^\mu_j\zeta^\mu_l\zeta^\nu_l\zeta^\nu_k), \tag{37}$$

where the links (jl) and (lk) are a μ-link and a ν-link, respectively. In the Majorana fermion representation, the three-site interactions read

$$i(\alpha^\mu_j\alpha^\mu_l)(\alpha^\nu_l\alpha^\nu_k) = iu^\mu_{jl}u^\nu_{kl}\lambda^4_j\lambda^4_k, \tag{38a}$$
$$i(\zeta^\mu_j\zeta^\mu_l)(\zeta^\nu_l\zeta^\nu_k) = iu^\mu_{jl}u^\nu_{kl}\lambda^5_j\lambda^5_k. \tag{38b}$$

As the Majorana operators λ^s_l do not appear explicitly in the right hand side of Eqs. (38), we can regard these perturbations as next-nearest-neighbor hopping operators for $\lambda^{4,5}_j$. We have a different type of three-site interactions in which different sets of Dirac matrices are used for two links:

$$\mathcal{H}_x = -\sum_{(jlk)} iK^x_{jlk}(\alpha^\mu_j\alpha^\mu_l\gamma^5_l\gamma^0_l\alpha^\nu_l\alpha^\nu_k - \zeta^\mu_j\zeta^\mu_l\gamma^5_l\gamma^0_l\zeta^\nu_l\zeta^\nu_k). \tag{39}$$

This yields another type of next-nearest-neighbor hopping term,

$$i(\alpha^\mu_j\alpha^\mu_l)\gamma^5_l\gamma^0_l(\zeta^\nu_l\zeta^\nu_k) = -iu^\mu_{jl}u^\nu_{kl}\lambda^4_j\lambda^5_k, \tag{40a}$$
$$i(\zeta^\mu_j\zeta^\mu_l)\gamma^5_l\gamma^0_l(\alpha^\nu_l\alpha^\nu_k) = iu^\mu_{jl}u^\nu_{kl}\lambda^5_j\lambda^4_k. \tag{40b}$$

The summations in Eqs. (37) and (39) are over any three neighboring sites which belong to the same plaquette, including the three sites $(jl'k)$, in addition to (jlk), in Fig. 3. For the $\mathbb{Z}_2$ gauge fields satisfying the π-flux condition, Eq. (20), the product of $\mathbb{Z}_2$ gauge fields $u_{jl}u_{kl}$ in Eqs. (38) has the opposite sign compared to the product $u_{jl'}u_{kl'}$. We assume $K^z_{jlk} = -K^z_{jl'k}$ and $K^x_{jlk} = -K^x_{jl'k}$ so that the two paths give the same contributions. This leads to a vanishing next-nearest-neighbor hopping for 0-flux plaquettes.

To summarize, under the π-flux condition (20), we have the following two types of next-nearest-neighbor hopping Hamiltonian:

$$\mathcal{H}_z = -\sum_{j\in\mathrm{A}}\sum_{\alpha=1,2} iK^\alpha_z(\lambda^4_j\lambda^4_{j+a_\alpha} - \lambda^5_j\lambda^5_{j+a_\alpha}) + \sum_{j\in\mathrm{B}}\sum_{\alpha=1,2} iK^\alpha_z(\lambda^4_j\lambda^4_{j+a_\alpha} - \lambda^5_j\lambda^5_{j+a_\alpha}), \tag{41a}$$

$$\mathcal{H}_x = -\sum_{j\in\mathrm{A}}\sum_{\alpha=1,2} iK^\alpha_x(\lambda^4_j\lambda^5_{j+a_\alpha} + \lambda^5_j\lambda^4_{j+a_\alpha}) + \sum_{j\in\mathrm{B}}\sum_{\alpha=1,2} iK^\alpha_x(\lambda^4_j\lambda^5_{j+a_\alpha} + \lambda^5_j\lambda^4_{j+a_\alpha}), \tag{41b}$$

where the parameters $K^{1,2}_{x,z}$ are hopping matrix elements. The subscript $j + a_\alpha$ denotes the site located at $\boldsymbol{r}_j + \boldsymbol{a}_\alpha$

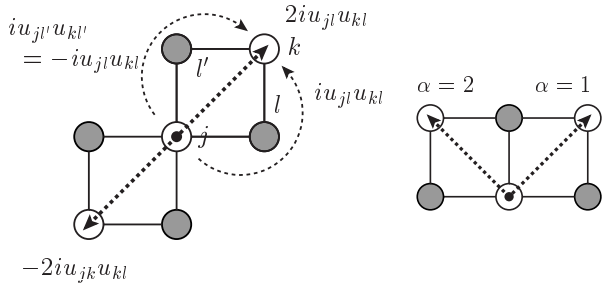

FIG. 3. Four-spin interaction terms. Left: The $\mathbb{Z}_2$ gauge fields obtained from the two paths connecting next-nearest-neighbor sites. Right: Two directions are labelled by $\alpha = 1, 2$, respectively.

with $\boldsymbol{a}_1 = (1, 1)$ and $\boldsymbol{a}_2 = (-1, 1)$. The two vectors $\boldsymbol{a}_{1,2}$ correspond to the two directions of next-nearest-neighbor hopping labelled by $\alpha = 1, 2$ in Fig. 3. We shall see that the next-nearest-neighbor hopping terms of the form

$$i(\lambda_j^4\lambda_k^4 - \lambda_j^5\lambda_k^5) \quad \text{and} \quad i(\lambda_j^4\lambda_k^5 + \lambda_j^5\lambda_k^4) \tag{42}$$

are invariant under time-reversal transformation which is defined in the next subsection.

Fourier transformation of Eqs. (41a) and (41b) yields

$$\mathcal{H}_z = \sum_{\boldsymbol{q}} \Theta_z(\boldsymbol{q})(a^4_{-\boldsymbol{q}}a^4_{\boldsymbol{q}} - b^4_{-\boldsymbol{q}}b^4_{\boldsymbol{q}} - a^5_{-\boldsymbol{q}}a^5_{\boldsymbol{q}} + b^5_{-\boldsymbol{q}}b^5_{\boldsymbol{q}}), \tag{43a}$$

$$\mathcal{H}_x = \sum_{\boldsymbol{q}} \Theta_x(\boldsymbol{q})(a^4_{-\boldsymbol{q}}a^5_{\boldsymbol{q}} - b^4_{-\boldsymbol{q}}b^5_{\boldsymbol{q}} + a^5_{-\boldsymbol{q}}a^4_{\boldsymbol{q}} - b^5_{-\boldsymbol{q}}b^4_{\boldsymbol{q}}), \tag{43b}$$

where

$$\Theta_i(\boldsymbol{q}) = K_i^1 \sin(q_x + q_y) + K_i^2 \sin(-q_x + q_y) \tag{44}$$

for $i = z, x$. The total Hamiltonian can be written as

$$\mathcal{H} = \mathcal{H}_0 + \mathcal{H}_z + \mathcal{H}_x = \sum_{\boldsymbol{q}} \psi^\dagger_{\boldsymbol{q}} \chi(\boldsymbol{q}) \psi_{\boldsymbol{q}}, \tag{45}$$

where

$$\psi_{\boldsymbol{q}} = \begin{pmatrix} a^4_{\boldsymbol{q}} \\ b^4_{\boldsymbol{q}} \\ a^5_{\boldsymbol{q}} \\ b^5_{\boldsymbol{q}} \end{pmatrix} \tag{46}$$

and

$$\begin{aligned}\chi(\boldsymbol{q}) &= \begin{pmatrix} \Theta_z & i\Phi & \Theta_x & 0 \\ -i\Phi^* & -\Theta_z & 0 & -\Theta_x \\ \Theta_x & 0 & -\Theta_z & i\Phi \\ 0 & -\Theta_x & -i\Phi^* & \Theta_z \end{pmatrix} \\ &= -\operatorname{Re}[\Phi(\boldsymbol{q})]\, c^y \otimes s^0 - \operatorname{Im}[\Phi(\boldsymbol{q})]\, c^x \otimes s^0 \\ &\quad + \Theta_z(\boldsymbol{q})\, c^z \otimes s^z + \Theta_x(\boldsymbol{q})\, c^z \otimes s^x. \end{aligned} \tag{47}$$

Here we have defined c^i $(i = x, y, z)$ as the Pauli matrices acting on the sublattice indices (a, b), and s^i as those on the Majorana flavors $(4, 5)$. The matrix s^0 is the 2×2 unit matrix in the Majorana flavor space. The Hamiltonian in the momentum space $\chi(\boldsymbol{q})$ is invariant under the translation by reciprocal lattice vectors, $\boldsymbol{G} = (\pm\pi, \pi)$. The eigenenergies are $\pm\varepsilon_{\boldsymbol{q}}$, where

$$\varepsilon_{\boldsymbol{q}} = \sqrt{|\Phi(\boldsymbol{q})|^2 + [\Theta_z(\boldsymbol{q})]^2 + [\Theta_x(\boldsymbol{q})]^2}. \tag{48}$$

Each energy level, for a given $\boldsymbol{q}$ has two-fold degeneracy.

We have seen in Sec. II D that the gapless phase of Hamiltonian $\mathcal{H}_0$ has two Dirac points at $\boldsymbol{q} = \boldsymbol{q}_i$ where $\Phi(\boldsymbol{q}_i) = 0$. Non-vanishing matrix elements $\Theta_x(\boldsymbol{q})$ and $\Theta_z(\boldsymbol{q})$ at the Dirac points give a band gap. Hence the gapless phase is turned into a gapped phase by including the three-spin interaction or next-nearest-neighbor hopping interactions $\mathcal{H}_z$ and $\mathcal{H}_x$.

Incidentally, both $\Theta_x(\boldsymbol{q})$ and $\Theta_z(\boldsymbol{q})$ vanish on the phase boundaries of the gapless and gapped phases of $\mathcal{H}_0$. Thus, the phase boundaries do not change upon addition of $\mathcal{H}_{z,x}$ to $\mathcal{H}_0$.

F. Symmetries

In this subsection, we consider symmetry properties of the Hamiltonian $\mathcal{H}$ in the Majorana fermion representation and show that it belongs to DIII symmetry class of the Altland-Zirnbauer classification.[22]

To this end, we begin with transforming the Majorana Hamiltonian $\mathcal{H}$ into Bogoliubov-de Gennes (BdG) Hamiltonian. We define fermion creation and annihilation operators on site j from the two flavors of Majorana fermions λ_j^4 and λ_j^5,

$$c_j = \frac{1}{2}(\lambda_j^4 + i\lambda_j^5), \qquad c_j^\dagger = \frac{1}{2}(\lambda_j^4 - i\lambda_j^5). \tag{49}$$

Their Fourier transforms are written as

$$\begin{pmatrix} A_{\boldsymbol{q}} \\ A^\dagger_{\boldsymbol{q}} \end{pmatrix} = \frac{1}{\sqrt{N}} \sum_j \begin{pmatrix} e^{-i\boldsymbol{q}\cdot\boldsymbol{r}_j} c_j \\ e^{i\boldsymbol{q}\cdot\boldsymbol{r}_j} c_j^\dagger \end{pmatrix}, \tag{50a}$$

for the A sublattice ($j \in$ A), and

$$\begin{pmatrix} B_{\boldsymbol{q}} \\ B^\dagger_{\boldsymbol{q}} \end{pmatrix} = \frac{1}{\sqrt{N}} \sum_k \begin{pmatrix} e^{-i\boldsymbol{q}\cdot(\boldsymbol{r}_k + \boldsymbol{e}_1)} c_k \\ e^{i\boldsymbol{q}\cdot(\boldsymbol{r}_k + \boldsymbol{e}_1)} c_k^\dagger \end{pmatrix}, \tag{50b}$$

for the B sublattice ($k \in$ B). The Nambu field for the complex fermion is defined by

$$\Psi_{\boldsymbol{q}} = \begin{pmatrix} A_{\boldsymbol{q}} \\ B_{\boldsymbol{q}} \\ A^\dagger_{-\boldsymbol{q}} \\ B^\dagger_{-\boldsymbol{q}} \end{pmatrix} \tag{51}$$

and is related to $\psi_{\boldsymbol{q}}$ in Eq. (46) by the unitary transformation,

$$\psi_{\boldsymbol{q}} = U\Psi_{\boldsymbol{q}}, \tag{52}$$

where the unitary matrix U is given by

$$U = \frac{1}{\sqrt{2}} \begin{pmatrix} 1 & 0 & 1 & 0 \\ 0 & 1 & 0 & 1 \\ -i & 0 & i & 0 \\ 0 & -i & 0 & i \end{pmatrix}. \tag{53}$$

Then the Hamiltonian $\mathcal{H}$ can be written in the form of BdG Hamiltonian,

$$\mathcal{H} = \sum_{\boldsymbol{q}} \Psi_{\boldsymbol{q}}^\dagger \tilde{\chi}(\boldsymbol{q}) \Psi_{\boldsymbol{q}}, \tag{54}$$

where

$$\begin{aligned} \tilde{\chi}(\boldsymbol{q}) =& U^\dagger \chi(\boldsymbol{q}) U \\ =& \begin{pmatrix} 0 & i\Phi(\boldsymbol{q}) & \Theta(\boldsymbol{q}) & 0 \\ -i\Phi^*(\boldsymbol{q}) & 0 & 0 & -\Theta(\boldsymbol{q}) \\ \Theta^*(\boldsymbol{q}) & 0 & 0 & i\Phi(\boldsymbol{q}) \\ 0 & -\Theta^*(\boldsymbol{q}) & -i\Phi^*(\boldsymbol{q}) & 0 \end{pmatrix} \qquad (55) \\ =& -\operatorname{Re}[\Phi(\boldsymbol{q})] c^y \otimes t^0 - \operatorname{Im}[\Phi(\boldsymbol{q})] c^x \otimes t^0 \\ &+ \operatorname{Re}[\Theta(\boldsymbol{q})] c^z \otimes t^x - \operatorname{Im}[\Theta(\boldsymbol{q})] c^z \otimes t^y \qquad (56) \end{aligned}$$

with $\Theta(\boldsymbol{q})$ defined by

$$\Theta(\boldsymbol{q}) = \Theta_z(\boldsymbol{q}) + i\Theta_x(\boldsymbol{q}). \tag{57}$$

The Pauli matrices t^i $(i = x, y, z)$ and the 2×2 unit matrix t^0 act on the Nambu indices.

We are ready to discuss symmetries of our model in terms of the BdG Hamiltonian $\tilde{\chi}(\boldsymbol{q})$. Under the particle-hole transformation generated by $\mathcal{P} = t^x \mathcal{K}$, where $\mathcal{K}$ is complex conjugation operator, the BdG Hamiltonian changes its sign,

$$t^x \tilde{\chi}^T(-\boldsymbol{q}) t^x = -\tilde{\chi}(\boldsymbol{q}). \tag{58}$$

We note that $\mathcal{P}^2 = +1$.

The BdG Hamiltonian is invariant under time-reversal transformation

$$i(c^z \otimes t^y) \tilde{\chi}^T(-\boldsymbol{q})(-i)(c^z \otimes t^y) = \tilde{\chi}(\boldsymbol{q}). \tag{59}$$

The time-reversal operator $\mathcal{T} = c^z \otimes i t^y \mathcal{K}$ obeys $\mathcal{T}^2 = -1$.

We conclude from these symmetry properties that the BdG Hamiltonian $\tilde{\chi}$ belongs to symmetry class DIII; see, e.g., Table 1 in Ref. 9. It is known from the classification theory of topological insulators and superconductors[7–9] that gapped ground states of class DIII Hamiltonian in two spatial dimensions can be classified by a $\mathbb{Z}_2$ index; see, e.g., Table 3 in Ref. 9.

The product of particle-hole and time-reversal transformations, $\mathcal{TP}$, yields

$$(c^z \otimes t^z) \tilde{\chi}(\boldsymbol{q}) (c^z \otimes t^z) = -\tilde{\chi}(\boldsymbol{q}), \tag{60}$$

i.e., $\tilde{\chi}(\boldsymbol{q})$ anticommutes with $c^z \otimes t^z$. In the basis where $c^z \otimes t^z$ is $\operatorname{diag}(1, 1, -1, -1)$, the BdG Hamiltonian is written in the off-diagonal form,

$$\tilde{\chi}_D(\boldsymbol{q}) = I_{24} \tilde{\chi}(\boldsymbol{q}) I_{24} = \begin{pmatrix} 0 & D(\boldsymbol{q}) \\ D^\dagger(\boldsymbol{q}) & 0 \end{pmatrix}, \tag{61}$$

where

$$I_{24} = \begin{pmatrix} 1 & 0 & 0 & 0 \\ 0 & 0 & 0 & 1 \\ 0 & 0 & 1 & 0 \\ 0 & 1 & 0 & 0 \end{pmatrix} \tag{62}$$

and

$$D(\boldsymbol{q}) = \begin{pmatrix} \Theta(\boldsymbol{q}) & i\Phi(\boldsymbol{q}) \\ -i\Phi^*(\boldsymbol{q}) & -\Theta^*(\boldsymbol{q}) \end{pmatrix}. \tag{63}$$

Since I_{24} and t^x commute, we find from Eqs. (58) and (61) that $D(\boldsymbol{q})$ satisfies the skew relation

$$D^T(-\boldsymbol{q}) = -D(\boldsymbol{q}). \tag{64}$$

Since $I_{24} c^z \otimes i t^y I_{24} = i t^y$, the time-reversal operator for $\tilde{\chi}_D(\boldsymbol{q})$ is $\mathcal{T} = i t^y \mathcal{K}$.

The symmetry relations in Eqs. (58) and (59) lead to symmetry relations for the Majorana Hamiltonian $\chi(\boldsymbol{q})$ through the unitary transformation. The particle-hole symmetry relation implies

$$\chi^T(-\boldsymbol{q}) = -\chi(\boldsymbol{q}), \tag{65}$$

while the time-reversal symmetry gives

$$c^z \otimes (is^y) \chi^T(-\boldsymbol{q}) c^z \otimes (-is^y) = \chi(\boldsymbol{q}). \tag{66}$$

It follows from these relations that $\chi(\boldsymbol{q})$ anticommutes with $c^z \otimes s^y$,

$$(c^z \otimes s^y) \chi(\boldsymbol{q}) (c^z \otimes s^y) = -\chi(\boldsymbol{q}). \tag{67}$$

We note that the time-reversal operator $c^z \otimes (is^y)\mathcal{K}$ in Eq. (66) is consistent with that for the Majorana operators [Eqs. (21a) and (21b)].

We return to the time-reversal symmetry of the next-nearest-neighbor hopping terms, Eq. (42). When the time-reversal operator $\mathcal{T} = c^z \otimes (is^y)\mathcal{K}$ is applied to the $\lambda_j^s \lambda_k^{s'}$, c^z does nothing since both sites j and k are on the same sublattice, while is^y interchanges $s = 4$ and $s = 5$ with a factor of -1 $(+1)$ for $s \neq s'$ $(s = s')$. Thus,

$$\mathcal{T} i \lambda_j^4 \lambda_k^5 \mathcal{T}^{-1} = i \lambda_j^5 \lambda_k^4, \tag{68a}$$

$$\mathcal{T} i \lambda_j^4 \lambda_k^4 \mathcal{T}^{-1} = -i \lambda_j^5 \lambda_k^5, \tag{68b}$$

and the hopping terms in Eq. (42) are invariant under the time-reversal transformation.

III. PHASES AND TOPOLOGICAL INVARIANT

In this section we show the existence of a Kramers' pair of Majorana edge modes in the topological phase and define a $\mathbb{Z}_2$ index that distinguishes between the topologically nontrivial and trivial phases.

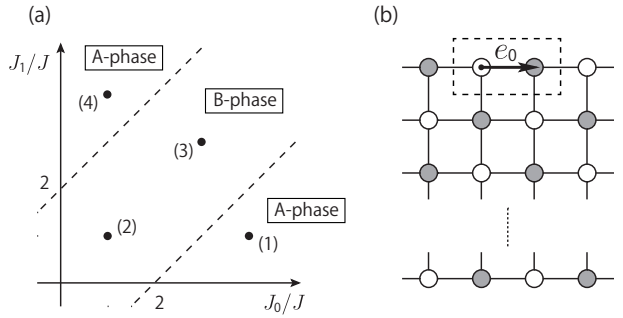

FIG. 4. (a) Phase diagram in the $J_0/J - J_1/J$ plane. The region between the dashed lines $J_1 = J_0 \pm 2J$, including the isotropic point $J_1 = J_0 = J$, is the gapless phase when the next-nearest-neighbor hopping terms are absent ("B-phase"). The gapless phase is turned into a topologically nontrivial phase when the second-nearest-neighbor hopping is turned on. Both the gapped phases for $J_1 > J_0 + 2J$ and for $J_1 < J_0 - 2J$ remain topologically trivial upon including the second-nearest-neighbor hopping terms ("A-phase"). The numbered solid circles indicate the parameter sets for which the energy spectra are calculated and shown in Fig. 5. (b) Strip geometry with edges along the vector $\boldsymbol{e}_0$.

A. Energy spectrum

We examine the energy spectrum of Majorana fermions by varying two coupling constants J_0 and J_1 while the others are kept fixed as $J_2 = J_3 = J$ and $K_x^1 = K_x^2 = K_z^1 = K_z^2 = K$, for simplicity. All coupling constants are taken to be positive. We set the $\mathbb{Z}_2$ gauge fields $u^\mu = (-1, 1, 1, 1)$ as before.

When $K = 0$, the eigenvalues of $\chi(\boldsymbol{q})$ are given by

$$E_{\boldsymbol{q}} = \pm|\Phi(\boldsymbol{q})| = \pm\left|\sum_{\mu=0}^{3} J_\mu u^\mu e^{i\boldsymbol{q}\cdot\boldsymbol{e}_\mu}\right|. \tag{69}$$

When $J_0 - 2J < J_1 < J_0 + 2J$ the positive and negative energy bands touch at two Dirac points ("B-phase" in Fig. 4). For example, in the isotropic case $J_0 = J_1 = J$ the Dirac points are located at $\boldsymbol{q} = (0, \pm\pi/2)$. As we approach the phase boundaries $J_1 - J_0 = \pm 2J$, the two Dirac points come closer to each other and eventually merge at $\boldsymbol{q} = (0, 0)$ for $J_1 = J_0 - 2J$ and at $\boldsymbol{q} = (\pi/2, \pi/2)$ for $J_1 = J_0 + 2J$. On the other hand, in the gapped phase where $J_0 - 2J > J_1$ or $J_0 + 2J < J_1$, there is an energy gap between positive and negative energy bands ("A-phase").

The effective Hamiltonian around the Dirac points is a Dirac Hamiltonian with the mass terms proportional to the next-nearest-neighbor hopping K. Note that $\Theta(\boldsymbol{q})$ vanishes at $\boldsymbol{q} = (0, 0)$ and $(\pi/2, \pi/2)$. This means that the band gap is closed at $J_1 = J_0 \pm 2J$ even in the presence of the next-nearest-neighbor hopping. Thus the parameter space $J_0/J - J_1/J$ is divided into three regions by the phase boundaries $J_1 = J_0 \pm 2J$ (the dashed lines in Fig. 4).

We have numerically diagonalized the Majorana tight-binding model $\mathcal{H}_0 + \mathcal{H}_z + \mathcal{H}_x$ for the strip geometry, shown in Fig. 4(b), where the edges are parallel to the link vectors $\boldsymbol{e}_0$ and $\boldsymbol{e}_2$. The energy spectra of $\mathcal{H}_0$ in the strip geometry are shown in Fig. 5 for $J_\mu/J = (4, 1, 1, 1)$ [(1a) and (1b)], $J_\mu/J = (1, 1, 1, 1)$ [(2a) and (2b)], $J_\mu/J = (3, 3, 1, 1)$ [(3a) and (3b)], and $J_\mu/J = (1, 4, 1, 1)$ [(4a) and (4b)]. We have chosen two values for the next-nearest-neighbor hopping: $K = 0$ [(1a),(2a),(3a),(4a)] and $K/J = 0.15$ [(1b),(2b),(3b),(4b)].

Without the next-nearest-neighbor hopping terms ($K = 0$), flat bands appear exactly at zero energy in the region $J_0 - 2J < J_1$. In the gapless phase (B-phase), the energy spectrum shows two Dirac points at time-reversal symmetric momenta, and the doubly degenerate zero-energy flat bands connect these two points through $q_x = 0$ (i.e., not through $q_x = \pi/2$); see Fig. 5 (3a). In the gapped phase (A-phase) where $J_0 + 2J < J_1$, the bulk bands are fully gapped, and the flat bands are extended in the whole Brillouin zone [Fig. 5 (4a)].

The existence of these zero-energy flat bands can be explained by a topological argument.[27] When $K = 0$, λ^4 and λ^5 decouples in our model. The bulk Hamiltonian for λ^4 (or λ^5) has the form

$$h(\boldsymbol{q}) = \boldsymbol{R}(\boldsymbol{q}) \cdot \boldsymbol{\sigma}, \tag{70}$$

where $\boldsymbol{R}(\boldsymbol{q})$ is a two-dimensional vector,

$$\boldsymbol{R}(\boldsymbol{q}) = \begin{pmatrix} -\mathrm{Im}[\widetilde{\Phi}(\boldsymbol{q})] \\ -\mathrm{Re}[\widetilde{\Phi}(\boldsymbol{q})] \end{pmatrix} \tag{71}$$

with

$$\widetilde{\Phi}(\boldsymbol{q}) = e^{-iq_x}(-J_0 e^{iq_x} + J_1 e^{iq_y} + J_2 e^{-iq_x} + J_3 e^{-iq_y}), \tag{72}$$

$\boldsymbol{q}$ is the wave vector in the first Brillouin zone, and $\boldsymbol{\sigma} = (\sigma^x, \sigma^y)$. In Eq. (72) $\widetilde{\Phi}(\boldsymbol{q})$ has the phase factor e^{-iq_x} [cf. $\Phi(\boldsymbol{q})$ in Eq. (36)], because we have chosen the unit cell depicted by the dashed line in Fig. 4(b) which is commensurate with the presence of the boundary. Note that $h(\boldsymbol{q})$ has chiral symmetry, $\{h(\boldsymbol{q}), \sigma^z\} = 0$. When we fix q_x, $h(\boldsymbol{q})|_{q_x}$ can be regarded as a one-dimensional Hamiltonian with wave number q_y in the direction perpendicular to the edge. The one-dimensional Hamiltonian has zero-energy edge modes if a loop trajectory that $\boldsymbol{R}(\boldsymbol{q})|_{q_x}$ draws as q_y is varied encloses the origin $\boldsymbol{R} = 0$ in the two-dimensional parameter space $\boldsymbol{R} = (R^x, R^y)$.[27,28] The number of zero-energy edge modes is given by the winding number of the loop and can change only when the loop touches the origin, i.e., when a band gap closes. For a fixed q_x, the loop is an ellipse described by the equation

$$\frac{[R^x + (J_0 + J_2)\sin q_x]^2}{(J_1 - J_3)^2} + \frac{[R^y + (J_0 - J_2)\cos q_x]^2}{(J_1 + J_3)^2} = 1. \tag{73}$$

[In deriving Eq. (73) we have ignored the phase factor e^{-iq_x} in $\widetilde{\Phi}(\boldsymbol{q})$, since it does not change the winding number.] The flat band appears when the origin $\boldsymbol{R} = 0$ is

inside the ellipse, i.e., when q_x satisfies

$$\sin^2 q_x < \frac{(J_1-J_3)^2[(J_1+J_3)^2-(J_0-J_2)^2]}{4(J_0J_1+J_2J_3)(J_0J_3+J_1J_2)}. \quad (74)$$

In the phase diagram in Fig. 4(a), the right-hand side of Eq. (74) is larger than unity for $J_1 > J_0 + 2J$ (A-phase in the upper side), while it is less than zero for $J_1 < J_0 + 2J$ (A-phase in the lower side), which explains the spectra shown in Fig. 5 (1a) and (4a). Otherwise, when $J_0 - 2J < J_1 < J_0 + 2J$ (B-phase), the right-hand side of (74) takes an intermediate value between 0 and 1, corresponding to the Fig. 5 (2a) and (3a).

When the next-nearest-neighbor terms are included ($K \neq 0$), the bulk bands are gapped in the whole region of the A- and B-phases. Then the flat bands are split from the zero energy, except at the time-reversal invariant momenta $q_x = 0, \pi/2$. Hence the edge modes in the B-phase have a single zero-energy point in the first Brillouin zone [Fig. 5 (2b) and (3b)], since the flat bands for $K = 0$ pass through $q_x = 0$ only, while those in the A-phase have an even number of zero-energy points [Fig. 5 (1b) and (4b)].

B. $\mathbb{Z}_2$ index

The phase with topologically protected edge states is characterized by a nontrivial $\mathbb{Z}_2$ index calculated in the bulk. The $\mathbb{Z}_2$ index introduced by Kane and Mele[29,30] for time-reversal invariant band insulators in class AII is defined through the matrix

$$w_{ij}(\boldsymbol{q}) = \langle u_i(-\boldsymbol{q})|\mathcal{T}u_j(\boldsymbol{q})\rangle, \quad (75)$$

where $|u_j(\boldsymbol{q})\rangle$ is the single-particle Bloch wave function in the i-th filled bands. The $\mathbb{Z}_2$ invariant ν is then given by

$$\nu = \prod_{\boldsymbol{q}:\mathrm{TRIM}} \frac{\sqrt{\det[w(\boldsymbol{q})]}}{\mathrm{Pf}[w(\boldsymbol{q})]}, \quad (76)$$

where TRIM is the time-reversal invariant momenta in the Brillouin zone, $(0,0)$, $(\pi/2,\pi/2)$, $(0,\pi)$, and $(-\pi/2,\pi/2)$. The sign of the square root in the numerator is chosen to be continuous along the path connecting the four time-reversal invariant momenta. The topological phase of our model in class DIII can also be characterized by the $\mathbb{Z}_2$ index defined by Eq. (76).

For models in symmetry class DIII, the $\mathbb{Z}_2$ index becomes apparent when Hamiltonian is expressed in the off-diagonal form by utilizing the chiral symmetry. Let us introduce the operator Q that has the eigenvalue $+1$ (-1) for the states in empty (filled) band of the BdG Hamiltonian $\tilde{\chi}$. When $\tilde{\chi}(\boldsymbol{q})$ is diagonalized as $\tilde{\chi} = V\mathrm{diag}(\epsilon_1, \epsilon_2, \cdots, -\epsilon_1, -\epsilon_2, \cdots)V^{-1}$ with a unitary matrix V, the operator Q is given by

$$Q = V\mathrm{diag}(1, 1, \cdots, -1, -1, \cdots)V^{-1}. \quad (77)$$

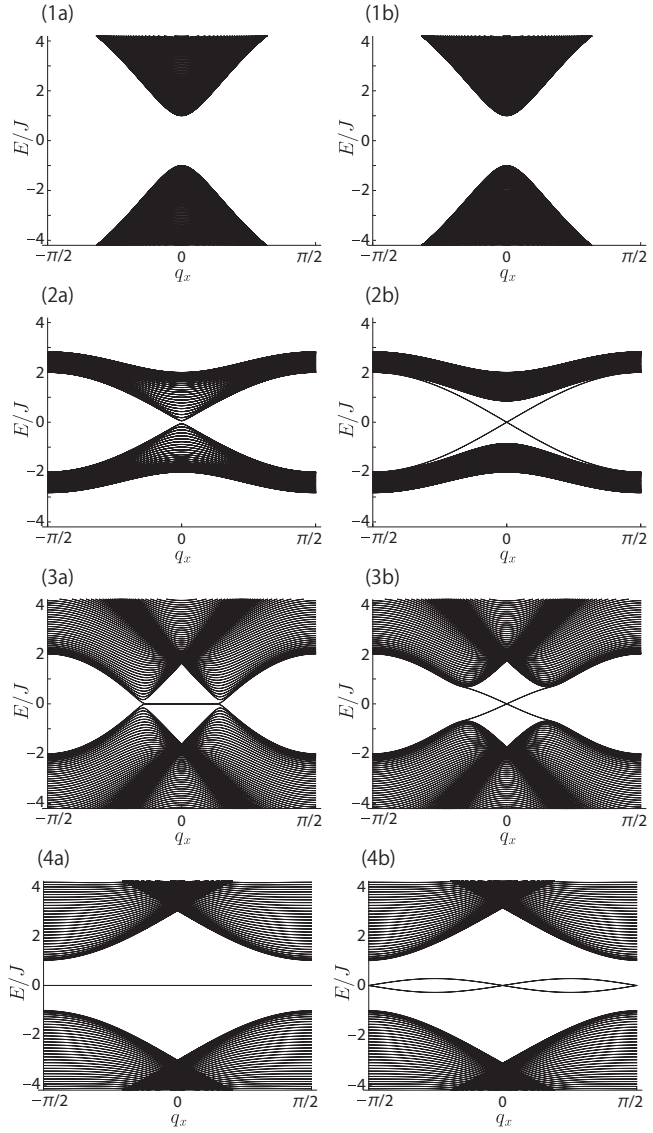

FIG. 5. Energy spectra of the one-dimensional strip [Fig. 4(b)] as a function of the momentum along the edge. The energy spectra are calculated for the following parameter sets [see also Fig. 4(a)]: $J_\mu/J = (4,1,1,1)$ in (1a) and (1b); $J_\mu/J = (1,1,1,1)$ in (2a) and (2b); $J_\mu/J = (3,3,1,1)$ in (3a) and (3b); $J_\mu/J = (1,4,1,1)$ in (4a) and (4b). The $\mathbb{Z}_2$ gauge are fixed as $u^\mu = (-1,1,1,1)$. The second-nearest-neighbor hopping $K_i^\alpha = 0$ ($\alpha = 1,2$ and $i = z,x$) in the left figures [(1a), (2a), (3a), (4a)], $K_i^\alpha/J = 0.15$ in the right figures [(1b), (2b), (3b), (4b)].

In the basis where $\tilde{\chi}(\boldsymbol{q})$ takes the off-diagonal form of Eq. (61), the operator Q also takes the form

$$Q(\boldsymbol{q}) = \begin{pmatrix} 0 & q(\boldsymbol{q}) \\ q^\dagger(\boldsymbol{q}) & 0 \end{pmatrix}. \quad (78)$$

The off-diagonal component $q(\boldsymbol{q})$ satisfies the relations $q^T(-\boldsymbol{q}) = -q(\boldsymbol{q})$ [so does $D(\boldsymbol{q})$] and $q^\dagger q = qq^\dagger = I$ (from $Q^2 = I$), where I is a unit matrix. In this basis the

operator Q is related to the BdG Hamiltonian $\tilde{\chi}$ by

$$Q(\boldsymbol{q}) = \frac{1}{\varepsilon_{\boldsymbol{q}}}\tilde{\chi}_D(\boldsymbol{q}) \tag{79}$$

with $\varepsilon_{\boldsymbol{q}}$ defined in Eq. (48).

The eigenvectors of Q in Eq. (78) are given by

$$u_{a\pm}(\boldsymbol{q}) = \frac{1}{\sqrt{2}}\begin{pmatrix} n_a \\ \pm q^\dagger(\boldsymbol{q}) n_a \end{pmatrix} \qquad (a = 1, 2), \tag{80}$$

where $\pm$ indicates the eigenvalue ± 1 (i.e., empty and filled bands), and n_a are unit vectors,

$$n_1 = \begin{pmatrix} 1 \\ 0 \end{pmatrix}, \qquad n_2 = \begin{pmatrix} 0 \\ 1 \end{pmatrix}. \tag{81}$$

Since the eigenspace of the operator Q of the eigenvalue -1 is the same as the Hilbert space that spanned by the filled bands of the BdG Hamiltonian, the $\mathbb{Z}_2$ index calculated with the vectors in Eq. (80) is equal to that calculated for the original BdG Hamiltonian.

Applying the time-reversal operator $\mathcal{T} = it^y\mathcal{K}$ to the eigenvector of the filled states given in Eq. (80) yields

$$\mathcal{T}|u_{a-}(\boldsymbol{q})\rangle = \frac{1}{\sqrt{2}}\begin{pmatrix} -q^T(\boldsymbol{q}) n_a \\ -n_a \end{pmatrix}. \tag{82}$$

The matrix w is then obtained as

$$w_{ab}(\boldsymbol{q}) = \langle u_{a-}(-\boldsymbol{q})|\mathcal{T}u_{b-}(\boldsymbol{q})\rangle = -q_{ba}(\boldsymbol{q}). \tag{83}$$

It then follows from Eqs. (61), (63), and (79) that

$$w(\boldsymbol{q}) = \frac{1}{\varepsilon_{\boldsymbol{q}}}\begin{pmatrix} \Theta(\boldsymbol{q}) & -i\Phi^*(\boldsymbol{q}) \\ i\Phi(\boldsymbol{q}) & -\Theta^*(\boldsymbol{q}) \end{pmatrix}. \tag{84}$$

Note that $\det[w(\boldsymbol{q})] = -1$ in the whole Brillouin zone, and that $w(\boldsymbol{q})$ becomes a purely imaginary antisymmetric matrix at the TRIM. Hence the $\mathbb{Z}_2$ index in Eq. (76) is reduced to

$$\nu = \prod_{\boldsymbol{q}:\mathrm{TRIM}} \mathrm{sgn}[\Phi(\boldsymbol{q})]. \tag{85}$$

At the TRIM we have

$$\Phi(0,0) = -J_0 + J_1 + J_2 + J_3, \tag{86a}$$
$$\Phi(0,\pi) = J_0 + J_1 - J_2 + J_3, \tag{86b}$$
$$\Phi(\pi/2,\pi/2) = J_0 - J_1 + J_2 + J_3, \tag{86c}$$
$$\Phi(-\pi/2,\pi/2) = -J_0 - J_1 - J_2 + J_3. \tag{86d}$$

The isotropic point, $J_\mu = J$, has $\nu = -1$ and is thus a topologically nontrivial state. In the limits where one of J_μ is much larger than the other three, $\nu = +1$ and the ground state is topologically trivial. These results are in agreement with the numerical results presented in Sec. III A. The presence or absence of helical Majorana edge states is dictated by the $\mathbb{Z}_2$ index ν.

At the phase boundaries between the topologically nontrivial phase and trivial phases, $\Phi(\boldsymbol{q})$ vanishes at least at one of the TRIM. Using Eqs. (86), we arrive at the phase diagram shown in Fig. 2, in which the shaded regions are topologically trivial phases and the rest is a topological phase (except on the phase boundaries).

IV. EDGE STATES AND SPIN CORRELATION FUNCTION

In this section we examine spin correlations of the ground state of the model, especially spin correlation functions along the edge of the two-dimensional system. The edge states appear in time-reversal pairs and form the helical Majorana edge modes as in the time reversal helical p-wave superconductors.[7] Spin correlation functions are calculated for these helical edge states.

Before proceeding to the calculation of correlation functions, we examine which operators have non-vanishing expectation values in the ground state. Operators can vanish due to two reasons: the projection operator and the constants of motion. The former one restricts non-vanishing operators to be the product of an even number of the Majorana operators on each site, because

$$\frac{1+D_j}{2}\lambda_j^p\frac{1+D_j}{2} = \frac{1+D_j}{2}\frac{1-D_j}{2}\lambda_j^p = 0, \tag{87}$$

where $p = 0, \ldots, 5$. The latter one implies that non-vanishing operators can contain the Majorana operators λ^μ with $\mu = 0, 1, 2, 3$ only in the form that does not flip the $\mathbb{Z}_2$ flux $\{\tilde{W}_p\}$, since such Majorana operators alter the $\mathbb{Z}_2$ gauge configuration:

$$u_{jk}^\mu\lambda_j^\mu = -\lambda_j^\mu u_{jk}^\mu \quad (\mu = 0, 1, 2, 3), \tag{88}$$
$$u_{jk}\lambda_j^4 = \lambda_j^4 u_{jk}, \qquad u_{jk}\lambda_j^5 = \lambda_j^5 u_{jk}, \tag{89}$$

and the projection operator does not flip the flux. These conditions can be restated as follows: non-vanishing operators for the ground state $|\mathrm{GS}\rangle$ of the γ matrix Hamiltonian are

1. $\mathbb{Z}_2$ gauge operators on closed strings of links,
2. $\mathbb{Z}_2$ gauge operators on open strings of links, each string having either λ_j^4 or λ_j^5 at the both ends,
3. $i\lambda_j^4\lambda_j^5$,
4. D_j,

and products thereof. The product of the $\mathbb{Z}_2$ gauge field operators on closed strings is rewritten as the product of the plaquette operators W_p and gives extra minus sign, since the plaquette operators are the integrals of motion for both the Majorana Hamiltonian and the γ matrix Hamiltonian. The correlation of operators which do not satisfy the above conditions does not extend beyond the nearest neighbor.

Here we consider the two-point correlation function of a local spin operator, which is a single-site operator, i.e., an operator that does not have a "string" composed of a product of operators. The only non-trivial single-site Hermitian operator that satisfies the above conditions is $i\lambda_j^4\lambda_j^5$. The term $i\lambda_j^4\lambda_j^5$ is equal to $i\gamma_j^5\gamma_j^0 = -i\alpha_j^\mu\zeta_j^\mu = (\sigma^0 \otimes \tau^2)_j$ in the γ matrix and Pauli

matrix representation, and is also written as $2c_j^\dagger c_j - 1$ in terms of the complex fermions (49). In the bulk, the two-point correlation function of $i\lambda_j^4\lambda_j^5$ is short-ranged since λ_j^4 and λ_j^5 are free Majorana fermion operators and the bulk is gapped. On the other hand, the correlation function of $i\lambda^4\lambda^5$ along the edge is expected to decay algebraically in the topological phase.

Let us consider the semi-infinite system with the edge along the x axis, and let q_x be the momentum along the edge, which is conserved. The fermion operators can be expanded as

$$\begin{aligned}\begin{pmatrix} a^4_{\boldsymbol{r}} \\ b^4_{\boldsymbol{r}} \\ a^5_{\boldsymbol{r}} \\ b^5_{\boldsymbol{r}} \end{pmatrix} &= \int_{-\pi/2}^{\pi/2} dq_x \sum_i e^{iq_x r_x} f_{q_x,i}(r_y)\xi_{q_x,i}, \\ &= \int_0^{\pi/2} dq_x \sum_i \left[e^{iq_x r_x} f_{q_x,i}(r_y)\xi_{q_x,i} \right. \\ &\qquad \left. + e^{-iq_x r_x} f^*_{q_x,i}(r_y)\xi^\dagger_{q_x,i}\right], \quad (90)\end{aligned}$$

where $\boldsymbol{r} = (r_x, r_y)$ labels unit cells which contain two sites (the semi-infinite system is defined for $r_y < 0$), $f_{q_x,i}(r_y)$ is the i-th exact single particle wavefunction with momentum q_x and energy $E_{q_x,i}$, and $f^*_{q_x,i}(r_y)$ is the particle-hole conjugate with $-E_{q_x,i}$; $\xi_{q_x,i}$ ($\xi^\dagger_{q_x,i}$) is the fermion annihilation (creation) operator associated with these levels. In computing the correlation function on the edge, the dominant contributions come only from the modes localized at the edge. Namely, the fermion operators near the edge are approximated by, at low energies,

$$\begin{aligned}\begin{pmatrix} a^4_{\boldsymbol{r}} \\ b^4_{\boldsymbol{r}} \\ a^5_{\boldsymbol{r}} \\ b^5_{\boldsymbol{r}} \end{pmatrix} &\simeq \int_0^{\pi/2} dq_x \left[e^{iq_x r_x} g_{+,q_x}(r_y)\gamma_{+,q_x} + \text{h.c.}\right] \\ &\quad + \int_0^{\pi/2} dq_x \left[e^{iq_x r_x} g_{-,q_x}(r_y)\gamma_{-,q_x} + \text{h.c.}\right], \end{aligned} \quad (91)$$

where $g_{\pm,q_x}(r_y)$ is the single-particle wavefunction of the left (right)-moving edge mode with momentum q_x, and $\gamma_{\pm,q_x}$ is the corresponding fermion annihilation operator. The edge contribution to the Hamiltonian is given by

$$\mathcal{H}_{\text{edge}} = \int_0^{\pi/2} dq_x E(q_x)\left(\gamma^\dagger_{+,q_x}\gamma_{+,q_x} - \gamma^\dagger_{-,q_x}\gamma_{-,q_x}\right). \quad (92)$$

The energy dispersion $E(q_x)$ for the edge mode is linear around a TRIM, $q_x = 0$, as shown by the numerics in Fig. 5.

At $q_x = 0$, the edge states are doubly degenerate at $E = 0$. For $K_z^1 = K_z^2 = K_z/2$ and $K_x^1 = K_x^2 = K_x/2$, the zero-energy eigen wavefunctions can be explicitly written as

$$g^\alpha_{q_x=0}(r_y) = (\Lambda_1^{r_y} - \Lambda_2^{r_y})\psi_0^\alpha \qquad (\alpha = 1, 2), \quad (93)$$

where $r_y < 0$ is an integer,

$$\psi_0^1 = \begin{pmatrix} -K_z \\ (J_1u^1 - J_3u^3)/2 \pm A \\ -K_x \\ 0 \end{pmatrix}, \quad (94)$$

$$\psi_0^2 = \begin{pmatrix} -K_x \\ 0 \\ K_z \\ (J_1u^1 - J_3u^3)/2 \pm A \end{pmatrix}, \quad (95)$$

with $A = \sqrt{K_z^2 + K_x^2 + (J_1u^1 - J_3u^3)^2/4}$, and $\Lambda_{1,2}$ are solutions of

$$\begin{aligned}&\left(\frac{J_1u^1 + J_3u^3}{2} \pm A\right)\Lambda^2 + \left(J_0u^0e^{iq} + J_2u^2e^{-iq}\right)\Lambda \\ &\quad + \left(\frac{J_1u^1 + J_3u^3}{2} \mp A\right) = 0. \end{aligned} \quad (96)$$

When $|\Lambda_1| > 1$ and $|\Lambda_2| > 1$, the wavefunctions (93) are normalizable and localized near the edges. Such solutions of Λ exist when

$$\left|\frac{J_1u^1 + J_3u^3}{2} \pm A\right| < \left|\frac{J_1u^1 + J_3u^3}{2} \mp A\right| \quad (97)$$

and

$$(J_0u^0 + J_2u^2)^2 > (J_1u^1 + J_3u^3)^2, \quad (98)$$

where all J_μ are assumed to be positive. The former condition (97) determines which signs to be taken. The latter condition (98) coincides with the region in Fig. 4 where there are zero-energy edge states at $q_x = 0$. In lowest order in q_x, the two-fold degeneracy of the zero modes is lifted; the energy dispersion near $q_x = 0$ is $E = \pm vq$, with the velocity

$$v = \sqrt{(J_0u^2 - J_2u^2)^2(K_z^2 + K_x^2)/A^2}. \quad (99)$$

In lowest order in q_x, the eigen wavefunctions $g^{(0)}_{\pm,q_x}$ are linear combinations of $g^1_{q_x=0}$ and $g^2_{q_x=0}$.

From the edge theory with a linear dispersion at low energies, one can immediately see the (equal-time) two-point correlation function of the Majorana fermion operators decay along the edge as $\langle\lambda^s(r_x)\lambda^{s'}(r'_x)\rangle \sim (r_x - r'_x)^{-1}$. The two-point correlation function of the operator $i\gamma^5\gamma^0 = \sigma^0 \otimes \tau^2 = i\lambda_j^4\lambda_j^5$ can be represented, using the Wick's theorem, as

$$\begin{aligned}\langle(\sigma^0 \otimes \tau^2)_r\,(\sigma^0 \otimes \tau^2)_{r'}\rangle &= \langle(i\lambda^4\lambda^5)_r\,(i\lambda^4\lambda^5)_{r'}\rangle \\ &\sim \frac{C(r_y, r'_y)}{(r_x - r'_x)^2}, \end{aligned} \quad (100)$$

where $C(r_y, r'_y)$ is a function of r_y and r'_y which is determined by the wavefunction of the edge modes $g^{(0)}_{\pm,q_x}$ and decays exponentially into the bulk.

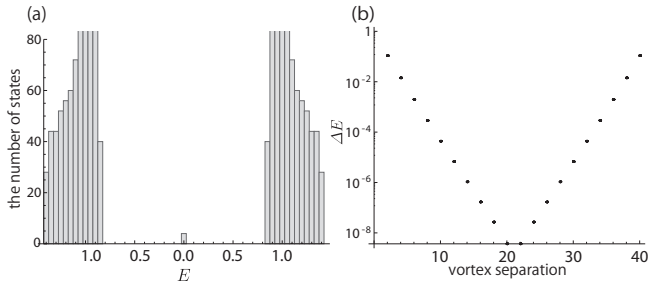

FIG. 6. (a) The number of states in the topological phase for 20×42 system with a pair of vortices separated by 20 lattice spacings. Periodic boundary conditions are imposed in the x and y directions. The parameters in the Hamiltonian are $J^\mu = 1$ and $K^{1,2}_{x,z} = 0.3$. (b) The energy difference ΔE between the positive and negative energy eigenvalues of bound states, as a function of the distance between the vortices.

V. VORTEX BOUND STATES

In this section we discuss vortex bound states in the topological phase. An isolated vortex in a topological superconductor can accommodate a topologically protected zero-energy Majorana state.[31] The time-reversal symmetry of our model implies that there are two such Majorana zero-energy states which form a Kramers' doublet.

In our model a vortex corresponds to a plaquette with a 0-flux in the π-flux background. Such 0-flux excitations always appear in pair since the total flux is a conserved quantity modulo 2π. As we noted above, each vortex should have two Majorana bound states. To confirm the number of bound Majorana states, we have numerically diagonalized Hamiltonian in the topological phase (the B phase in Fig. 4) for the system size of 20×42 sites, in which two 0-flux plaquettes are placed along the y direction. We have imposed periodic boundary conditions in the x and y directions and set the parameters as $J^\mu = 1$ and $K^{1,2}_{x,z} = 0.3$.

Figure 6(a) shows the number of eigenstates when two vortices are separated by 20 lattice spacings. We find four nearly-zero-energy states inside the bulk gap, i.e., two states per vortex. The energy eigenvalues of these midgap states are $\pm\Delta E/2$, each energy eigenvalue being two-fold degenerate. Figure 6(b) shows ΔE as a function of the distance r between the two vortices. The dependence of ΔE on r is symmetric about $r = 21$, because of the periodic boundary conditions imposed. The clear exponential dependence on r ($r < 21$) confirms that the energy difference ΔE is due to a small overlap of exponential tails of wave functions bound to the two vortices.

VI. EXTENDED KITAEV MODEL ON THE ONE-DIMENSIONAL LATTICE

In this section we study the extended Kitaev model on the cylinder geometry, i.e., the ladder with two sets of rungs. The sites on the ladder are divided into A and B sublattices, shown as open and filled circles in Fig. 7, respectively. The μ-links are defined as in the two-dimensional case.

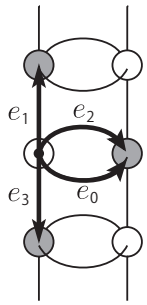

FIG. 7. One-dimensional system on a two-leg cylindrical lattice.

We consider the nearest-neighbor interaction Hamiltonian

$$\mathcal{H}_{\rm 1D} = -\sum_{\mu=0}^{3} J_\mu \sum_{\mu\text{-links}} (\alpha_j^\mu \alpha_k^\mu + \zeta_j^\mu \zeta_k^\mu). \tag{101}$$

We use the Majorana fermion representation of the Dirac matrices (17), and combine λ^4 and λ^5 to make complex fermions as in Eq. (49), and take the Fourier transform of the Majorana operators

$$A_q = \frac{1}{\sqrt{L}} \sum_{j\in \rm A} e^{-iqy_j} (\lambda_j^4 + i\lambda_j^5)/2, \tag{102a}$$

$$B_q = \frac{1}{\sqrt{L}} \sum_{k\in \rm B} e^{-iqy_k} (\lambda_k^4 + i\lambda_k^5)/2, \tag{102b}$$

where L is the length of the cylinder, y_j and y_k are the positions of the sites in the vertical coordinate. The Hamiltonian in the momentum space is then given by

$$\begin{aligned}\mathcal{H}_{\rm 1D} &= i\sum_{\mu=0}^{3} J_\mu \sum_{\mu\text{-links}} u_{jk}^\mu (\lambda_j^4 \lambda_k^4 + \lambda_j^5 \lambda_k^5) \\ &= \sum_q \Psi_q^\dagger \chi_{\rm 1D} \Psi_q,\end{aligned} \tag{103}$$

where the spinor Ψ_q is

$$\Psi_q = \begin{pmatrix} A_q \\ B_q \\ A_{-q}^\dagger \\ B_{-q}^\dagger \end{pmatrix}, \tag{104}$$

and

$$\chi_{\rm 1D} = \begin{pmatrix} 0 & i\Phi(q) & 0 & 0 \\ -i\Phi^*(q) & 0 & 0 & 0 \\ 0 & 0 & 0 & i\Phi(q) \\ 0 & 0 & -i\Phi^*(q) & 0 \end{pmatrix} \tag{105}$$

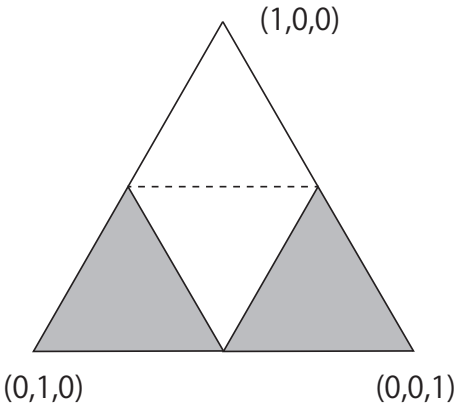

FIG. 8. Phase diagram of the one-dimensional cylindrical lattice model in the parameter space (J_0+J_2, J_1, J_3). The phase in which one of the horizontal bonds J_0 and J_2 is greater than the other three bonds is a topologically trivial phase. The shaded regions (tetrahedra) are a topological phase, where each end of the ladder has two-fold degenerate zero-energy Majorana states.

with

$$\Phi(q) = J_0 u^0 + J_1 u^1 e^{iq} + J_2 u^2 + J_3 u^3 e^{-iq}. \tag{106}$$

The eigenenergies of $\chi_{1\mathrm{D}}$ are $E = \pm|\Phi(q)|$ and each energy level is doubly degenerate. From the Lieb's theorem, the ground state is obtained for the $\mathbb{Z}_2$ gauge field configurations with π-flux per each square, i.e., when the condition $\mathrm{sgn}\,[(J_1u^1)(J_3u^3)(J_0u^0+J_2u^2)(J_0u^0+J_2u^2)] = -1$ is satisfied. Without loss of generality, we will work with the $\mathbb{Z}_2$ gauge $u^\mu = (1,-1,1,1)$. The ground-state energy is then a function of three parameters $J_0 + J_2$, J_1, and J_3. Even without the next-nearest neighbor interaction terms, the ground state is gapped except at the phase boundaries,

$$J_1 - J_3 = \pm(J_0 + J_2). \tag{107}$$

The phase diagram is depicted in Fig. 8.

We diagonalized numerically the Hamiltonian for a finite length system with open boundary condition in the leg direction. No midgap states are found if $J_1 - J_3 < J_0 + J_2$ and $J_1 - J_3 > -(J_0 + J_2)$ (non-shaded region in Fig. 8), while midgap states bound to each end are found when $J_1 - J_3 > J_0 + J_2$ and $J_1 - J_3 < -(J_0 + J_2)$ (shaded regions in Fig. 8). These midgap modes of Majorana fermions have two-fold degeneracy due to the time-reversal symmetry, or equivalently, spin 1/2 degrees of freedom bound on each edge.

The Hamiltonian of one-dimensional system (105) has the same symmetry as that of two-dimensional system (55). Thus the $\mathbb{Z}_2$ invariant is the product of

$$\frac{\sqrt{\det[w(q)]}}{\mathrm{Pf}[w(q)]} = \mathrm{sgn}[\Phi(q)] \tag{108}$$

at the TRIM in the one-dimensional Brillouin zone,

$$\Phi(0) = J_0 - J_1 + J_2 + J_3, \tag{109a}$$

$$\Phi(\pi) = J_0 + J_1 + J_2 - J_3. \tag{109b}$$

The phase boundaries obtained from the $\mathbb{Z}_2$ invariant coincides with those from numerics, which are already given in (107). Since the class DIII Hamiltonian (105) can be decomposed into two independent blocks, each of which is a member of class AIII, the $\mathbb{Z}_2$ invariant in this case coincides with the even-odd parity of the integral invariant (winding number) of class AIII for the blocks. In turn, the winding number can be obtained by drawing the loop trajectory in the parameter space defined by $\Phi(q)$ in Eq. (105) [see for discussion around Eq. (72)]; The product $\mathrm{sgn}[\Phi(0)]\mathrm{sgn}[\Phi(\pi)]$ (i.e., the $\mathbb{Z}_2$ invariant) then tells us that, when negative, the loop trajectory drawn by $\Phi(q)$ encloses the origin an odd number of times.

VII. CONCLUSIONS

In this paper, we have introduced a time-reversal symmetric two-dimensional quantum spin model in a topologically non-trivial gapped phase, as a γ-matrix extension of the Kitaev model on the square lattice. Through a fermion representation of the γ matrices, this model is equivalent to a time-reversal symmetric two-dimensional topological superconductor (i.e., a system in class DIII in the Altland-Zirnbauer classification). The Hamiltonian consists of nearest-neighbor interaction terms and next-nearest-neighbor interaction terms, all of which are transformed to free Majorana fermion hopping Hamiltonian with $\mathbb{Z}_2$ gauge field. In the parameter space of the Hamiltonian, topologically trivial ground states and non-trivial ones are realized. We have confirmed that these two phases are distinguished by the $\mathbb{Z}_2$ topological invariant.

We have shown using both numerical and analytical methods the existence of topologically protected, a Kramers' pair of Majorana edge modes, which is a hallmark of a time-reversal symmetric topological superconductor. A local operator of a product of two flavors of Majorana operators, which is equivalent to the density operator of a complex fermion, has a nonvanishing correlation that decays in inverse-square of the distance along the edge and decays exponentially in the bulk. We have also shown numerically that a vortex of the $\mathbb{Z}_2$ gauge field hosts a Kramers' pair of zero-energy Majorana states.

On the one-dimensional ladder lattice, we have constructed the same type of extended Kitaev model. Similarly to the square lattice case, two topologically distinct types of ground states appear in the phase diagram, which are characterized by the $\mathbb{Z}_2$ topological invariant.

ACKNOWLEDGMENTS

This work was supported in part by Grant-in-Aid for JSPS Fellows (No. 227763) and Grant-in-Aid for Scientific Research (No. 21540332) from the Japan Society for

the Promotion of Science and by the National Science Foundation under Grant No. NSF PHY05-51164. AF and SR are grateful to the Kavli Institute for Theoretical Physics for its hospitality, where this paper was completed.

Appendix: Jordan-Wigner transformation of the gamma matrix Kitaev model

In this appendix, we present a solution to the Kitaev-type model (7), in terms of the Jordan-Wigner transformation, following the solution of the original Kitaev model by Jordan-Wigner transformation.[32–35]

1. Jordan-Wigner transformation of the Dirac matrices

As a first step, we note that it is possible to represent the Dirac matrices for a given site in terms of two complex fermions c_1 and c_2 as

$$\begin{aligned} \alpha^0 &= (c_1 + c_1^\dagger), \qquad \alpha^1 = (c_2 + c_2^\dagger), \\ \alpha^2 &= (c_1 - c_1^\dagger)/i, \qquad \alpha^3 = (c_2 - c_2^\dagger)/i, \end{aligned} \tag{A.1}$$

where $\{c_1, c_1^\dagger\} = \{c_2, c_2^\dagger\} = 1$, and $\{c_1, c_2\} = \{c_1, c_2^\dagger\} = 0$. The right-hand side of four equations in (A.1) are Majorana fermion operators. Similarly, using $\zeta^\mu = \gamma^5\gamma^0\alpha^\mu$,

$$\begin{aligned} \zeta^0 &= e^{i\pi n_2}(c_1 - c_1^\dagger)/i, \qquad \zeta^1 = e^{i\pi n_1}(c_2 - c_2^\dagger)/i, \\ \zeta^2 &= -e^{i\pi n_2}(c_1 + c_1^\dagger), \qquad \zeta^3 = -e^{i\pi n_1}(c_2 + c_2^\dagger), \end{aligned} \tag{A.2}$$

$$i\gamma^5\gamma^0 = \sigma^0 \otimes \tau^y = e^{i\pi(n_1+n_2)}, \tag{A.3}$$

where $n_1 = c_1^\dagger c_1$, $n_2 = c_2^\dagger c_2$, and we have used the relation $e^{i\pi n_a} = 1 - 2n_a = -(c_a + c_a^\dagger)(c_a - c_a^\dagger)$.

For the Kitaev-type model (7), we need to prepare a set of two complex fermions c_{1j} and c_{2j} for each site labeled by j. Accordingly, one needs to introduce string operators to ensure commutation relations for operators sitting on different sites. At fist, we consider the string operators for 0-th and second components of the Dirac matrices, which contain single Majorana operators made of c_1. Since 0-links and 2-links horizontally connect neighboring sites (Fig. 1), we define an order of sites on the two-dimensional lattice that runs horizontally:

$$\begin{aligned} &(x_1, y_1) < (x_2, y_2) \Leftrightarrow \\ &\quad y_1 > y_2 \text{ or } (y_1 = y_2 \text{ and } x_1 < x_2), \end{aligned} \tag{A.4}$$

where x and y are the two-dimensional coordinates (Fig. 1). Multiplying the right-hand side of the 0-th and second components in Eqs. (A.1) and (A.2) by string operators of products of $e^{i\pi n_1}$ with the order (A.4) [Fig. 1(a)],

$$U_j = \prod_{j>k} e^{i\pi n_{1k}}, \tag{A.5}$$

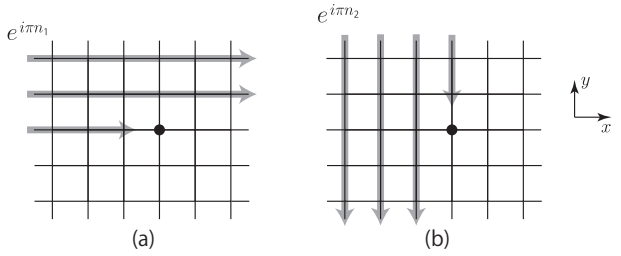

FIG. 9. String operators of Jordan-Wigner fermions that represent Dirac matrices for (a) Majorana fermion made of c_1 (U_j), and (b) those made of c_2 (V_j).

makes these operators commute between different sites.

Next, we can also introduce string operators for the first and third component, with another order of sites on the same two-dimensional lattice [Fig. 1(b)]

$$\begin{aligned} &(x_1, y_1) < (x_2, y_2) \Leftrightarrow \\ &\quad x_1 < x_2 \text{ or } (x_1 = x_2 \text{ and } y_1 > y_2), \end{aligned} \tag{A.6}$$

as

$$V_j = \prod_{j>k} e^{i\pi n_{2k}}. \tag{A.7}$$

The latter string operator (A.7) ensures commutativity of the first and third component of Dirac matrix on different sites. Finally, in order for Jordan-Wigner fermion representation of all four component of Dirac matrix to be bosonic, the first and third component of Dirac matrix on a site j is multiplied by string operator that runs all the sites besides j:

$$W_j = \prod_{k(\neq j)} e^{i\pi n_{1k}}. \tag{A.8}$$

As a result, we obtain the Jordan-Wigner fermion representation of Dirac matrices as

$$\begin{aligned} \alpha_j^0 &= (c_{1j} + c_{1j}^\dagger)U_j, \\ \alpha_j^1 &= (c_{2j} + c_{2j}^\dagger)V_jW_j, \\ \alpha_j^2 &= -i(c_{1j} - c_{1j}^\dagger)U_j, \\ \alpha_j^3 &= -i(c_{2j} - c_{2j}^\dagger)V_jW_j, \end{aligned} \tag{A.9}$$

and

$$\begin{aligned} \zeta_j^0 &= -i(c_{1j} - c_{1j}^\dagger)e^{i\pi n_{2j}}U_j, \\ \zeta_j^1 &= -i(c_{2j} - c_{2j}^\dagger)e^{i\pi n_{1j}}V_jW_j, \\ \zeta_j^2 &= -(c_{1j} + c_{1j}^\dagger)e^{i\pi n_{2j}}U_j, \\ \zeta_j^3 &= -(c_{2j} + c_{2j}^\dagger)e^{i\pi n_{1j}}V_jW_j. \end{aligned} \tag{A.10}$$

2. Jordan-Wigner transformation of the γ matrix Kitaev model

Utilizing the Jordan-Wigner fermion representation of Dirac matrices, we can transform our spin model to a free Majorana fermion model, without redundancy.

On 0-links, since $j \in$ A and $k \in$ B connected by a 0-link have the order $j < k$ defined in (A.4), the nearest-neighbor interaction terms are transformed as follows.

$$\begin{aligned}\alpha_j^0\alpha_k^0 &= (c_{1j}+c_{1j}^\dagger)U_j(c_{1k}+c_{1k}^\dagger)U_k\\ &= -(c_{1j}-c_{1j}^\dagger)(c_{1k}+c_{1k}^\dagger),\\ \zeta_j^0\zeta_k^0 &= -(c_{1j}-c_{1j}^\dagger)e^{i\pi n_{2j}}U_j(c_{1k}-c_{1k}^\dagger)e^{i\pi n_{2k}}U_k\\ &= \left[(c_{1j}+c_{1j}^\dagger)e^{i\pi n_{2j}}\right]\left[(c_{1k}-c_{1k}^\dagger)e^{i\pi n_{2k}}\right].\end{aligned}$$

Considering the order of $j \in$ A and $k \in$ B in the string operators ((A.4) and (A.6)), nearest-neighbor interaction terms on the other three links are similarly transformed as

$$\begin{aligned}\alpha_j^1\alpha_k^1 &= \left[(c_{2j}+c_{2j}^\dagger)e^{i\pi n_{1j}}\right]\left[(c_{2k}-c_{2k}^\dagger)/i\, e^{i\pi n_{1k}}\right],\\ \zeta_j^1\zeta_k^1 &= -(c_{2j}-c_{2j}^\dagger)(c_{2k}+c_{2k}^\dagger),\end{aligned}$$

$$\begin{aligned}\alpha_j^2\alpha_k^2 &= -(c_{1j}-c_{1j}^\dagger)(c_{1k}+c_{1k}^\dagger),\\ \zeta_j^2\zeta_k^2 &= \left[(c_{1j}+c_{1j}^\dagger)e^{i\pi n_{2j}}\right]\left[(c_{1k}-c_{1k}^\dagger)e^{i\pi n_{2k}}\right],\end{aligned}$$

$$\begin{aligned}\alpha_j^3\alpha_k^3 &= \left[(c_{2j}+c_{2j}^\dagger)e^{i\pi n_{1j}}\right]\left[(c_{2k}-c_{2k}^\dagger)e^{i\pi n_{1k}}\right],\\ \zeta_j^3\zeta_k^3 &= -(c_{2j}-c_{2j}^\dagger)(c_{2k}+c_{2k}^\dagger).\end{aligned}$$

Here we introduce two Majorana fermion operators on each site as

$$\begin{cases}\lambda_j^4 &= -(c_{2j}+c_{2j}^\dagger)e^{i\pi n_{1j}},\\ \lambda_j^5 &= -i(c_{2j}-c_{2j}^\dagger),\end{cases} \tag{A.11}$$

$$\begin{cases}\lambda_k^4 &= -i(c_{2k}-c_{2k}^\dagger)e^{i\pi n_{1k}},\\ \lambda_k^5 &= c_{2k}+c_{2k}^\dagger,\end{cases} \tag{A.12}$$

where $j \in$ A and $k \in$ B. Those Majorana fermion operators transform the nearest-neighbor interaction terms on 1-links and 3-links to free Majorana hopping terms without $\mathbb{Z}_2$ gauge operators, as

$$\begin{aligned}&-\sum_{\mu=1,3}J_\mu\sum_{\mu\text{-links}}(\alpha_j^\mu\alpha_k^\mu+\zeta_j^\mu\zeta_k^\mu)\\ &\quad= i\sum_{\mu=1,3}J_\mu\sum_{\mu\text{-links}}(\lambda_j^4\lambda_k^4+\lambda_j^5\lambda_k^5).\end{aligned} \tag{A.13}$$

Majorana fermions in Eq. (A.12) also transform the nearest-neighbor interaction terms on 0-links and 2-links to free Majorana hopping terms, however in this case, with $\mathbb{Z}_2$ gauge operators:

$$\begin{aligned}&-\sum_{\mu=0,2}J_\mu\sum_{\mu\text{-links}}(\alpha_j^\mu\alpha_k^\mu+\zeta_j^\mu\zeta_k^\mu)\\ &\quad= i\sum_{\mu=0,2}J_\mu\sum_{\mu\text{-links}}u_{jk}(\lambda_j^4\lambda_k^4+\lambda_j^5\lambda_k^5),\end{aligned} \tag{A.14}$$

where u_{jk} are $\mathbb{Z}_2$ gauge operators of the form

$$u_{jk} = -(c_{1j}+c_{1j}^\dagger)(c_{2j}+c_{2j}^\dagger)(c_{1k}-c_{1k}^\dagger)(c_{2k}-c_{2k}^\dagger). \tag{A.15}$$

The $\mathbb{Z}_2$ gauge operators commute with each other, and also commute with $\lambda_j^4, \lambda_k^4, \lambda_j^5, \lambda_k^5$:

$$[u_{jk}, u_{lm}] = 0, \tag{A.16}$$

$$[u_{jk}, \lambda_l^4] = [u_{jk}, \lambda_l^5] = 0. \tag{A.17}$$

Consequently, we obtain the Jordan-Wigner transformation of the γ matrix Kitaev model as

$$\begin{aligned}\mathcal{H} = i&\left(\sum_{0\text{-links}}J_0u_{jk}+\sum_{1\text{-links}}J_1+\sum_{2\text{-links}}J_2u_{jk}+\sum_{0\text{-links}}J_3\right)\\ &\times(\lambda_j^4\lambda_k^4+\lambda_j^5\lambda_k^5).\end{aligned} \tag{A.18}$$

In this representation, the number of the $\mathbb{Z}_2$ gauge operators reduces to the half of that in the local Majorana representation (18), and therefore there is no redundancy in this fermionic representation. If we consider the periodic boundary condition, string operators appear in the Hamiltonian in connecting both edges, as discussed in the case of the Kitaev model.[33]

* rnakai@vortex.c.u-tokyo.ac.jp

[1] X.-G. Wen, Int. J. Mod. Phys. B **4**, 239 (1990); X.-G. Wen and Q. Niu, Phys. Rev. B **41**, 9377 (1990); X.-G. Wen, Adv. Phys. **44**, 405 (1995).

[2] See, e.g., X. Chen, Z.-C. Gu, Z.-X. Liu, and X.-G. Wen, arXiv:1106.4772.

[3] Z.-C. Gu and X.-G. Wen, Phys. Rev. B **80**, 155131 (2009).

[4] F. Pollmann, A. M. Turner, E. Berg, and M. Oshikawa, Phys. Rev. B **81**, 064439 (2010).

[5] M. Z. Hasan and C. L. Kane, Rev. Mod. Phys. **82**, 3045 (2010).

[6] X.-L. Qi and S.-C. Zhang, Rev. Mod. Phys. **83**, 1057 (2011).

[7] A. P. Schnyder, S. Ryu, A. Furusaki, and A. W. W. Ludwig, Phys. Rev. B **78**, 195125 (2008); AIP Conf. Proc. **1134**, 10 (2009).

[8] A. Yu. Kitaev, AIP Conf. Proc. **1134**, 22 (2009).

[9] S. Ryu, A. P. Schnyder, A. Furusaki, and A. W. W. Ludwig, New J. Phys. **12**, 065010 (2010).

[10] See for example, B. A. Bernevig and S.-C. Zhang, Phys. Rev. Lett. **96**, 106802 (2006); M. Levin and A. Stern, Phys. Rev. Lett. **103**, 196803 (2009); J. Maciejko, X.-L. Qi, A. Karch, and S.-C. Zhang, Phys. Rev. Lett. **105**, 246809 (2010); B. Swingle, M. Barkeshli, J. McGreevy, and T. Senthil, Phys. Rev. B **83**, 195139 (2011); X.-L. Qi, Phys. Rev. Lett. **107**, 126803 (2011); T. Neupert, L. Santos, S. Ryu, C. Chamon, and C. Mudry, Phys. Rev. B **84**, 165107 (2011); M. Levin, F. J. Burnell, M. Koch-Janusz, and A. Stern, Phys. Rev. B **84**, 235145 (2011); T. Neupert, L. Santos, S. Ryu, C. Chamon, and C. Mudry, Phys. Rev. Lett. **108**, 046806 (2012), and references therein.

[11] I. Affleck, T. Kennedy, E. H. Lieb, and H. Tasaki, Phys. Rev. Lett. **59**, 799 (1987).

[12] D. S. Rokhsar and S. A. Kivelson, Phys. Rev. Lett. **61**, 2376 (1988).

[13] A. Yu. Kitaev, Ann. Phys. (N.Y.) **303**, 2 (2003).

[14] Michael Levin and Xiao-Gang Wen, Phys. Rev. B **67**, 245316 (2003).

[15] A. Kitaev, Ann. Phys. (N.Y.) **321**, 2 (2006).

[16] H. Yao and D.-H. Lee Phys. Rev. Lett. **107**, 087205 (2011).

[17] H. H. Lai and O. I. Motrunich, Phys. Rev. B **84**, 085141 (2011); **84**, 235148 (2011).

[18] G. A. Fiete, V. Chua, M. Kargarian, R. Lundgren, A. Ruegg, J. Wen, and V. Zyuzin, arXiv:1106.0013.

[19] S. Ryu, Phys. Rev. B **79**, 075124 (2009).

[20] C. Wu, D. Arovas, and H.-H. Hung, Phys. Rev. B **79**, 134427 (2009).

[21] H. Yao, S.-C. Zhang, and S. A. Kivelson, Phys. Rev. Lett. **102**, 217202 (2009).

[22] A. Altland and M. R. Zirnbauer, Phys. Rev. B **55**, 1142 (1997).

[23] C. Gils, S. Trebst, A. Kitaev, A. W. W. Ludwig, M. Troyer, and Z. Wang, Nature Physics **5**, 834 (2009).

[24] The gapless (algebraic spin liquid) phase in a similar model to ours is discussed in Ref. 21.

[25] C. Itzykson and J.-B. Zuber, *Quantum Field Theory* (McGraw-Hill, New York, 1980).

[26] E. H. Lieb, Phys. Rev. Lett. **73**, 2158 (1994).

[27] S. Ryu and Y. Hatsugai, Phys. Rev. Lett. **89**, 077002 (2002).

[28] In this case $h(\boldsymbol{q})$ can be continuously deformed to a simple one-dimensional chiral-symmetric Hamiltonian which obviously has zero-energy end states.

[29] C. L. Kane and E. J. Mele, Phys. Rev. Lett. **95**, 146802 (2005).

[30] L. Fu and C. L. Kane, Phys. Rev. B **74**, 195312 (2006).

[31] N. Read and D. Green, Phys. Rev. B **61**, 10267 (2000).

[32] X.-Y. Feng, G.-M. Zhang, and T. Xiang, Phys. Rev. Lett. **98**, 087204 (2007).

[33] H. Yao and S. A. Kivelson, Phys. Rev. Lett. **99**, 247203 (2007).

[34] H.-D. Chen and J. Hu, Phys. Rev. B **76**, 193101 (2007).

[35] H.-D. Chen and Z. Nussinov, J. Math. A: Math. Theor. **41**, 075001 (2008).